



HAL
open science

Cadmium isotope composition of the Earth's mantle inferred from analysis of oceanic basalts and komatiites

Gabriel Devos, Frédéric Moynier, John Creech, Deze Liu, Igor S Puchtel,
Martin Bizzarro

► **To cite this version:**

Gabriel Devos, Frédéric Moynier, John Creech, Deze Liu, Igor S Puchtel, et al.. Cadmium isotope composition of the Earth's mantle inferred from analysis of oceanic basalts and komatiites. *Chemical Geology*, 2024, 650, pp.121996. 10.1016/j.chemgeo.2024.121996 . hal-04520357

HAL Id: hal-04520357

<https://hal.science/hal-04520357>

Submitted on 25 Mar 2024

HAL is a multi-disciplinary open access archive for the deposit and dissemination of scientific research documents, whether they are published or not. The documents may come from teaching and research institutions in France or abroad, or from public or private research centers.

L'archive ouverte pluridisciplinaire **HAL**, est destinée au dépôt et à la diffusion de documents scientifiques de niveau recherche, publiés ou non, émanant des établissements d'enseignement et de recherche français ou étrangers, des laboratoires publics ou privés.

Cadmium isotope composition of the Earth's mantle inferred from analysis of oceanic basalts and komatiites

Gabriel Devos ^a, Frederic Moynier ^a, John Creech ^a, Deze Liu ^b,

Igor S. Puchtel ^c, and Martin Bizzarro ^{a,d}

^a Université Paris Cité, Institut de physique du globe de Paris, CNRS, F-75005 Paris, France

^b Department of Earth sciences, University of Oxford, South Parks Road, Oxford OX1 3AN, UK

^c Department of Geology, University of Maryland, College Park, MD 20742, USA

^d Centre for Star and Planet Formation, Globe Institute, University of Copenhagen, Øster Voldgade 5–7,
Copenhagen DK-1350, Denmark

Published in *Chemical Geology*

Vol 650, p 121996

DOI: <https://doi.org/10.1016/j.chemgeo.2024.121996>

Keywords: Cadmium stable isotopes; Cadmium double spike; MC-ICP-MS; Bulk Silicate Earth; mid-oceanic ridge basalts, komatiites

Abstract:

Cadmium stable isotope ratios can serve as valuable tracers for biological and geological processes, including nutrients sampling from the surrounding medium, volatilization events, and terrestrial differentiation. However, studies of the isotope fractionation occurring during geological processes require the characterization of the isotope compositions of the different terrestrial reservoirs. Notably, the cadmium isotopic composition of the Bulk Silicate Earth (BSE) is still a matter of debate. To address this issue, we present high-precision cadmium isotope data from a diverse set of samples, including mid-oceanic ridge basalts (MORB) and komatiites obtained using a ^{106}Cd - ^{111}Cd double spike system. We processed nine biological and geological reference materials (AGV-2, BCR-2, BHVO-2, BIR-1, COQ 1, GSP-2, NIST 2711, NOD-A-1, ERM BB 186) and two pure Cd solutions (AAS and ChemLab) to assess the accuracy and precision of the method.

Our study revealed that twenty-three MORB samples (including ten analyses from the literature) from the Atlantic, Indian, and Pacific oceans have a homogeneous cadmium isotopic composition. The weighted mean isotope composition for these samples, expressed as $\delta^{114}\text{Cd}$ (the permil deviation of the $^{114}\text{Cd}/^{110}\text{Cd}$ ratio from the NIST SRM 3108 Cd standard), is $0.07 \pm 0.10 \text{ ‰}$ (2SD, $n = 23$). We also studied twelve komatiite samples from the Abitibi (Superior Craton, Canada), Barberton (Kaapvaal Craton, South Africa), and Kostomuksha (Baltic Shield, Fennoscandia) greenstone belts to characterize the deep Archean mantle isotope composition. These samples, combined with four analyses from the literature (Pickard et al., 2022) exhibited isotopic compositions ranging from $-0.33 \pm 0.04 \text{ ‰}$ to $0.26 \pm 0.08 \text{ ‰}$. We observed a negative correlation between cadmium abundances and the degree of secondary alteration (measured by loss on ignition-LOI). For samples with low LOI ($\leq 6 \text{ wt.}\%$), the isotope compositions of komatiites are quite consistent. On the other hand, the samples with higher LOI (between 6 and 8.4 wt.%) tend to be more scattered and can have lighter isotope compositions. These

correlations suggest that, although Cd isotope compositions in komatiites are quite resilient to alteration, heavier Cd isotopes can be mobilized into secondary alteration fluids, driving altered samples toward isotopically lighter compositions. This implies that secondary alteration exerts an important control on the isotope compositions of komatiites. Therefore, only the Cd isotope compositions of the least altered komatiites (i.e., those with LOI \leq 6 wt.%) have been used as proxies for their mantle source isotope composition. These samples (two from the Abitibi greenstone belt, one from the Barberton greenstone belt, one from the Baltic shield and one from the Belingwe greenstone belt) gave a weighted mean isotope composition of 0.14 ± 0.18 ‰ (2SD, n = 5). No significant isotope variation was found between the pristine samples from each region, despite ages ranging from 3549 ± 99 Ma to 2713 ± 29 Ma, indicating a possible isotopic homogeneity (within the currently achievable precision) of the Archean mantle for Cd starting as early as 3.55 billion years ago. We determined a Cd isotope composition for the mantle by combining the data for mean MORB and komatiites. This gave a $\delta^{114}\text{Cd}$ value of 0.11 ± 0.10 ‰ (2SD, n = 28) for the Bulk Silicate Earth. This value is significantly heavier than previously proposed.

1. Introduction

Cadmium (Cd) is classified as a moderately volatile element (MVE) due to its low T_{50} (50 % condensation temperature under solar nebula conditions) of 502 K (Wood et al., 2019). Moderately volatile elements are characterized by unique depletion patterns found in terrestrial objects (Earth, Moon, Mars, rocky meteorites), when compared to the average composition of the solar system, as determined by elemental composition of the Sun's photosphere (and approximated by CI carbonaceous chondrites) (Braukmüller et al., 2019; McDonough, 2014; Steenstra et al., 2019; Wang et al., 2016). Stable isotopes of MVE such as Cd (Sands et al., 2001; Wang et al., 2016; Wombacher et al., 2003), Cu (Luck et al., 2005, 2003), Zn (Luck et al., 2005; Pringle et al., 2017), or Rb (Pringle and Moynier, 2017) have been used to provide insights into the origin of these variations in their abundances.

Being a group 12 element (same as Zn), Cd is characterized by divalent cations and siderophile (Kubik et al., 2021; Mahan et al., 2017; Marin et al., 2013; Steenstra et al., 2020) and chalcophile (Kiseeva and Wood, 2013; Wood et al., 2014) behaviors under core-forming conditions. It is also among the MVE with the lowest T_{50} (for comparison, T_{50} of Zn is 704K: Wood et al., 2019).

The study of Cd isotope composition started in the early XXth century (Aston, 1935, 1934; Nier, 1936; Stenvinkel and Svensson, 1935; Svensson, 1933). The development and improvement of thermal ionization mass spectrometers (TIMS) allowed the use of the Cd isotope system for elemental abundance determination by isotope dilution (Loss et al., 1984; Rosman and De Laeter, 1974a, 1974b) and for isotope composition determination using a ^{106}Cd - ^{111}Cd double spike (DS) (Rosman and De Laeter, 1975). Following this seminal work, a number of studies explored Cd isotope compositions of meteorites (Rosman et al., 1980b, 1980a; Rosman and De Laeter, 1988, 1978, 1976), using the DS method. These studies demonstrated that chondrites are characterized by significantly fractionated mass-dependent

isotope compositions compared to terrestrial materials, ranging from -2.1 to +2.8 ‰ per atomic mass unit (amu). Similarly, significant isotope variations (-2.3 to +6.3 ‰ per amu) were observed in Cd-poor lunar soils (Sands et al., 2001; Schediwy et al., 2006). However, unlike these extraterrestrial samples, most terrestrial rocks are characterized by smaller isotope variations (often less than ± 0.075 ‰ per amu: Chang et al., 2023; Horner et al., 2011, 2010; Liu et al., 2022; Lu et al., 2021; Murphy et al., 2016; Pallavicini et al., 2014; Pickard et al., 2022; Tan et al., 2020; Wombacher et al., 2003). From the 1980s to the 2000s, the external reproducibility achieved with TIMS, expressed as 2 standard deviations (2SD), was ranging from 0.06 to 2.9 ‰ per atomic mass unit, amu, (see Table 1). Thus, the precision of the measurements was then insufficient to distinguish between many terrestrial materials. Although a new generation of TIMS has been available since the 2000s, it was employed for the first time in 2009 for Cd isotope studies and significantly improved the overall reproducibility (see Figure 1), making the study of such samples accessible.

Table 1: Reproducibility of Cd isotope measurements in different studies and comparison between instrumental design and double spike formulae

Reference	Method	instrument	2 SD (‰ per amu)	
			min	max
Rosman and De Laeter (1975)	Constant run conditions	TIMS	0.800	1.600
Rosman et al. (1980) a	¹⁰⁶⁻¹¹¹ DS	TIMS	0.060	0.400
Rosman et al. (1980) b	¹⁰⁶⁻¹¹¹ DS	TIMS	0.300	1.000
Rosman and De Laeter (1988)	¹⁰⁶⁻¹¹¹ DS	TIMS	0.200	2.900
Sands et al. (2001)	¹⁰⁶⁻¹¹¹ DS	TIMS	0.200	0.800
Wombacher et al. (2003)	Ag-; Sb-normalization	ICP-MS	0.040	0.130
Cloquet et al. (2005)	SSB	ICP-MS	0.010	0.110
Schediwy et al. (2006)	¹⁰⁶⁻¹¹¹ DS	TIMS	0.200	15.000
*	*	*	*	0.900
Ripperger and Rehkämper (2007)	Ag normalization	ICP-MS	0.038	0.038
Ripperger and Rehkämper (2007)	¹¹⁰⁻¹¹¹ DS	ICP-MS	0.013	0.050
Schmitt et al. (2009) a	¹⁰⁶⁻¹⁰⁸ DS	Triton TIMS	0.006	0.028
Schmitt et al. (2009) b	¹⁰⁶⁻¹⁰⁸ DS	Triton TIMS	0.003	0.011
Horner et al. (2010)	¹¹¹⁻¹¹³ DS	ICP-MS	0.010	0.100
Horner et al. (2011)	¹¹¹⁻¹¹² DS	ICP-MS	0.033	0.070
Abouchami et al. (2014)	¹⁰⁶⁻¹⁰⁸ DS	Triton TIMS	0.004	0.017
Pallavicini et al. (2014)	SSB	ICP-MS	0.004	0.027
Wasylenki et al. (2014)	¹¹¹⁻¹¹⁶ DS	ICP-MS	0.015	0.045
Li et al. (2018)	¹¹¹⁻¹¹³ DS	ICP-MS	0.008	0.058
Tan et al. (2020)	¹¹¹⁻¹¹³ DS	ICP-MS	0.002	0.021
Borovička et al. (2020)	¹⁰⁶⁻¹¹⁶ DS	Triton TIMS	0.003	0.018
Liu et al. (2020)	¹¹¹⁻¹¹³ DS	ICP-MS	0.001	0.019
Druce et al. (2022)	¹¹⁰⁻¹¹¹ DS	ICP-MS	0.014	0.090
Pickard et al. (2022)	¹¹¹⁻¹¹³ DS	ICP-MS	0.008	0.035
Chang et al. (2023)	¹¹¹⁻¹¹³ DS	ICP-MS	0.003	0.015
Chang et al. (2023)	¹¹¹⁻¹¹³ DSSA - single	ICP-MS	0.006	0.062
Chang et al. (2023)	¹¹¹⁻¹¹³ DSSA - multi	ICP-MS	0.006	0.050
Peng et al. (2023)	¹¹¹⁻¹¹³ DS	ICP-MS	0.003	0.050
Pickard et al. (2023)	¹¹¹⁻¹¹³ DS	ICP-MS	0.010	0.020
This work	¹⁰⁶⁻¹¹¹ DS	ICP-MS	0.001	0.031

Reproducibilities are based on the reported 2SD for multiple measurements of pure standards or of samples. They are quoted in permil per atomic mass unit. "Min" and "Max" list the best and worst 2SD reported in the work, respectively. DS: double spike; SSB: standard sample bracketing; DSSA: double spike-standard addition. *Schediwy very high maximum 2SD was obtained at suboptimal concentrations for a very depleted sample (0.4 ng/g); its second worst 2SD gives a 0.900 ‰ per amu, much more representative of the overall precision achieved then. (Abouchami et al., 2014; Borovička et al., 2021; Chang et al., 2023; Cloquet et al., 2005; Druce et al., 2022a, 2022b; Horner et al., 2011, 2010; Li et al., 2018; Liu et al., 2020; Pallavicini et al., 2014; Peng et al., 2023; Pickard et al., 2023, 2022; Ripperger and Rehkämper, 2007; Rosman et al., 1980b,

1980a; Rosman and De Laeter, 1988, 1975; Sands et al., 2001; Schediwy et al., 2006; Schmitt et al., 2009a, 2009b; Tan et al., 2020; Wasylenki et al., 2014; Wombacher et al., 2003)

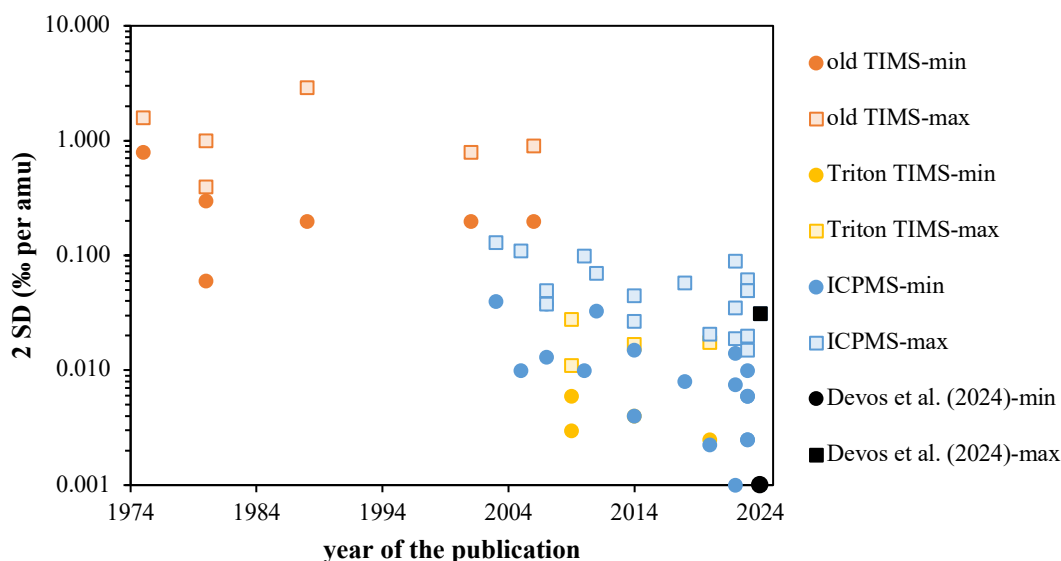


Figure 1: Evolution of the uncertainties reported in Cd isotope studies. The data represented here coincide with the one reported in Table 1. All uncertainties are normalized 2SD to obtain permil per amu deviations. The data are divided between three categories, depending on the mass spectrometer design utilized in the study. The introduction of a new mass spectrometer design usually coincides with a precision increase of at least one order of magnitude. “Min” and “Max” list the best and worst 2SD reported in the work, respectively. (Abouchami et al., 2014; Borovička et al., 2021; Chang et al., 2023; Cloquet et al., 2005; Druce et al., 2022a, 2022b; Horner et al., 2011, 2010; Li et al., 2018; Liu et al., 2020; Pallavicini et al., 2014; Peng et al., 2023; Pickard et al., 2023, 2022; Ripperger and Rehkämper, 2007; Rosman et al., 1980b, 1980a; Rosman and De Laeter, 1988, 1975; Sands et al., 2001; Schediwy et al., 2006; Schmitt et al., 2009a, 2009b; Tan et al., 2020; Wasylenki et al., 2014; Wombacher et al., 2003)

Many follow-up Cd studies employed these instruments (Abouchami et al., 2014, 2013; Borovička et al., 2021; Guinoiseau et al., 2018; Schmitt et al., 2009a) to analyze terrestrial samples, mostly using the ^{106}Cd - ^{108}Cd DS (Schmitt et al., 2009b). Concurrently, other researchers developed analytical methods for Cd isotope studies using inductively-coupled plasma mass-spectrometry (ICP-MS), following the pioneering work by Wombacher (2003), as a solution to the problem of low ionization efficiency of Cd encountered with TIMS. This new technique allowed for a similar or better precision than what was then achievable using TIMS, with 2SD ranging from 0.04 to 0.13 ‰ per amu (Wombacher et al., 2003). More recent TIMS (Borovička et al., 2021) and ICP-MS studies (Pickard et al., 2022) have demonstrated

comparable precisions, with 2SD ranging from 0.01 to 0.02 ‰ per amu. The ICP-MS technique was employed in studies characterizing the Cd isotopic compositions of extraterrestrial samples (Wombacher et al., 2008), volatilization-related isotope fractionation (Wombacher et al., 2004), isotope fractionation occurring during biological processes (Chang et al., 2023), or seawater cycles (Conway and John, 2015; Ripperger and Rehkämper, 2007), for tracing pollution (Cloquet et al., 2006; Robson et al., 2014; Wen et al., 2015; Zhu et al., 2018), reconstruction of paleo-ocean characteristics (Druce et al., 2022a, 2022b; Horner et al., 2011; Peng et al., 2023; Wasylenki et al., 2014), and study of Earth accretion history (Pickard et al., 2023, 2022).

Until 2013, no isotopic standard material was available, leading to multiple in-house reference materials being used simultaneously. Most recent studies use the NIST SRM (the US National Institute of Standards and Technology standard reference material) 3108 Cd standard solution (Abouchami et al., 2013). We will hereafter express Cd isotope compositions against this NIST 3108 standard as $\delta^{114}\text{Cd}$, defined as:

$$\delta^{114}\text{Cd} = \left[\frac{\left(\frac{{}^{114}\text{Cd}}{{}^{110}\text{Cd}} \right)_{\text{sample}}}{\left(\frac{{}^{114}\text{Cd}}{{}^{110}\text{Cd}} \right)_{\text{NIST SRM 3108}}} - 1 \right] \times 10^3$$

One of the main hindrances to wider Cd-oriented research using ICP-MS is the low abundances of Cd in most igneous rocks, with concentrations generally under 100 ng/g (ppb). Such low concentrations mean that samples have a high matrix over Cd ratio, which can result in problematic matrix effects and interferences during the analysis. Hence, extensive purification is usually undertaken, which could potentially cause Cd loss and significant isotope fractionation if the chemical yield is not close to 100 %. As a result, many studies focused on developing DS methods to correct for potential chemical and instrumental isotope fractionation (Ripperger and Rehkämper, 2007; Rosman and De Laeter, 1976; Schmitt et al., 2009b). With

6 stable isotopes (^{106}Cd , ^{108}Cd , ^{110}Cd , ^{111}Cd , ^{112}Cd and ^{114}Cd) and 2 long-lived radioactive isotopes (^{113}Cd and ^{116}Cd , $t_{1/2} > 10^{15}$ years) (Böhlke et al., 2005; Pritzkow et al., 2007), Cd is indeed highly suitable for double spike deconvolution, which requires at least four stable isotopes.

Despite this important analytical work, few widely available standard rock materials have been characterized for their Cd isotope compositions (Borovička et al., 2021; Chang et al., 2023; Cloquet et al., 2005; Horner et al., 2010; Li et al., 2018; Liu et al., 2020; Lu et al., 2021; Murphy et al., 2016; Pallavicini et al., 2014; Pickard et al., 2022; Tan et al., 2020; Wombacher et al., 2003), limiting inter-laboratory comparisons. Moreover, major processes affecting Cd isotope compositions have not yet been fully characterized. Notably, whether Cd isotopes are fractionated during igneous processes such as partial melting or fractional crystallization has never been tested, even though it is known to occur in some other isotopic systems, such as Zn, Ti, Fe, Zr, and Sn (Badullovich et al., 2017; Day et al., 2022; Inglis et al., 2019; Millet et al., 2016; Teng et al., 2008)

The Bulk Silicate Earth (BSE) is dominated (>99 wt. %) by the mantle (Yoder, 1995). Although the mantle Cd concentration is lower than that of the crust (38.3 ± 5.6 ppb, 80 ppb, and 126 ± 45 ppb for the mantle, continental crust, and oceanic crust, respectively: Rudnick and Gao, 2014; Wang et al., 2018; this study), it contains around 98 wt.% of the BSE Cd inventory. Thus, the Cd isotope composition of the BSE can be reliably approximated by that of the mantle.

The assumption of a well-mixed homogeneous mantle is known to be oversimplified, as the preservation of initial heterogeneities (Puchtel et al., 2018, 2016), and complex mixing processes of surficial materials in the deep mantle (Hofmann, 1997) contribute to present-day mantle heterogeneity (Helffrich and Wood, 2001; Lambart et al., 2019; Ohira et al., 2021; Van Keken et al., 2002). Generally, two major mantle reservoirs are usually considered: a more

heterogeneous lower mantle, which is the source of ocean island basalts (OIB) and a more homogeneous upper mantle. The latter reservoir is produced by the extraction of mid-oceanic ridge basalt (MORB) magmas enriched in incompatible trace elements and is, hence, called the DMM (depleted MORB mantle: Hirschmann and Stolper, 1996).

To date, only two estimates for the Cd isotope composition of the BSE are available, which are based on limited number of samples. These two estimates were obtained on three loesses (representing the continental crust), two MORB and two OIB (representing the DMM and the lower mantle respectively) (Schmitt et al., 2009a) ($\delta^{114}\text{Cd}_{\text{BSE}} = -0.04 \pm 0.02 \text{ ‰}$, 2SD, n = 7) and on four spinel lherzolite samples (Pickard et al., 2022) ($\delta^{114}\text{Cd}_{\text{BSE}} = -0.06 \pm 0.03 \text{ ‰}$, 2 SD, n = 4).

Using mantle-derived lavas to constrain the mantle isotope composition relies on the hypothesis that their isotope compositions mirror that of their source. This, however, may not always be the case as isotope fractionation during partial melting can make isotope compositions of melts drift away from that of their mantle sources. This may be especially so for compatible or moderately incompatible elements, for which a significant fraction of their original budgets remains in the mantle source during low degrees of partial melting. Such processes are known to produce small isotope fractionation for Zn, accounting for the isotope composition difference between OIB (2-10 % of melting), MORB (around 10 %), boninites (12-23 %) and komatiites (30 – 50 %) (Day et al., 2022). Cadmium is more incompatible than Zn, with MORB being 3 to 4 times Cd-richer than peridotites (Pickard et al., 2022; Wang et al., 2016; Witt-Eickschen et al., 2009; Yi et al., 2000) while they are only marginally enriched in Zn (Beunon et al., 2020; Day et al., 2022; Huang et al., 2018). Thus, we expect partial melting isotope fractionation to become insignificant at lower degrees of partial melting for Cd than for Zn. However, low degrees of melting should still affect the Cd isotope compositions of the lavas. This is why we chose to focus on igneous rocks to obtain an independent estimate

of the BSE isotopic composition for Cd to compare with the previous, peridotite-centered, value (Pickard et al., 2022).

Archean komatiites are lavas that sample from the heterogeneous deep mantle (Puchtel et al., 2022). They were chosen for this study because of the high degrees of partial melting that produced these melts (Herzberg, 1992), thus ensuring that no significant melting-related isotope fractionation occurs. The isotope compositions of the lavas can, however, be affected by olivine fractionation during magma differentiation, by Cd volatilization from the degassing melts (Yi et al., 2000) or by secondary processes. Since Cd has a low olivine-melt distribution coefficient (Richter et al., 2018), we do not expect that limited olivine fractionation would alter significantly the Cd isotope compositions of the melts. Moreover, the low viscosity of these magmas allows for a rapid ascent to the surface, with minimal magmatic differentiation before the eruption (Huppert et al., 1985).

The DMM composition can be determined by studying submarine-emplaced MORB. As submarine lavas are quenched upon emplacement, we do not expect significant Cd volatilization (Yi et al., 2000) or magma differentiation that could alter their original isotope compositions. Modern, unaltered samples of MORB are readily available. Thus, except if isotope fractionation is significant at the degrees of partial melting applicable to MORB formation, MORB isotope compositions should reflect that of the DMM.

The goal of this study is to obtain an accurate estimate of the Cd stable isotope composition of the BSE through the use of a ^{106}Cd - ^{111}Cd DS system. To achieve this goal, we analyzed a diverse set of samples, including MORB to represent the modern depleted mantle and komatiites to represent the Archean deep mantle. We selected MORB samples from the Atlantic, Indian, and Pacific oceans and komatiites from three distinct regions: Fennoscandia (Baltic Shield), Kaapvaal Craton (South Africa), and Superior Craton (Canada). Additionally, we included two Cretaceous Atlantic MORB samples to compare with their modern

equivalents. The komatiite samples span an age range of 800 million years (Ma), allowing us to investigate the evolution of the Cd isotopic composition of the Archean deep mantle over time. Compositions of OIB samples from the literature (Pickard et al., 2022; Schmitt et al., 2009a) will be included in our discussion of the Cd isotope composition of the modern deep mantle.

2. Samples

Fourteen bulk MORB samples were analyzed, with their sampling locations displayed in Figure 2 (She et al., 2023; Wood et al., 1979). Nine of these samples were collected from the Atlantic region, with five of these originating from the North mid-Atlantic ridge (NAR) and one from the South mid-Atlantic ridge (SAR). These six samples have zero age. One sample, DSDP 409, was identified as a vesicular basalt from the Reykjanes ridge and determined to be 2.3 Ma old (Wood et al., 1979). The last two Atlantic MORB, DSDP 51A-417A and DSDP 52-417D, were collected from the Cretaceous oceanic crust located to the East of the Caribbean. Although, DSDP 417A was collected just 400 m away from DSDP 417D, it has undergone extensive alteration, unlike DSDP 417D (Emmermann and Puchelt, 1980). In addition to these samples, one MORB from the central Indian ridge (CIR) (MD57 D6-7), one from the South-West Indian ridge (SWIR) (MD34 D1) and three from the East Pacific rise (EPR) (CYP 78 12-34, Sea Rise 1 DR04 301, and Sea Rise 2 DR03) were analyzed. Samples from Indian and Pacific oceans are regarded as modern in age.

Twelve komatiite samples were analyzed in this study, originating from five distinct locations: Boston Creek and Pyke Hill from the Superior Craton, Canada; Kostomuksha from the Fennoscandian Shield in northern Europe, and Schapenburg and Weltevreden, from the Kaapvaal Craton, South Africa. These samples are thought to have been derived from compositionally distinct mantle domains (Puchtel et al., 2022). Detailed descriptions, and major and trace element contents are available for all the samples, along with their ages (Byerly

et al., 2017; Chauvel et al., 1993; Connolly et al., 2011; Corfu and Noble, 1992; Puchtel et al., 2018, 2016, 2013, 2009, 2004, 1998), which range from 2713 to 3549 Ma. All samples, except for SCH-1.9, which is an olivine cumulate, are spinifex-textured komatiites. Samples from Kostomuksha and Weltevreden were derived from several lava flows, while the Boston Creek, Pyke Hill, and Schapenburg samples were collected within the same lava flows for each locality. Additionally, all komatiite samples have undergone varying degrees of serpentinization and metamorphism.

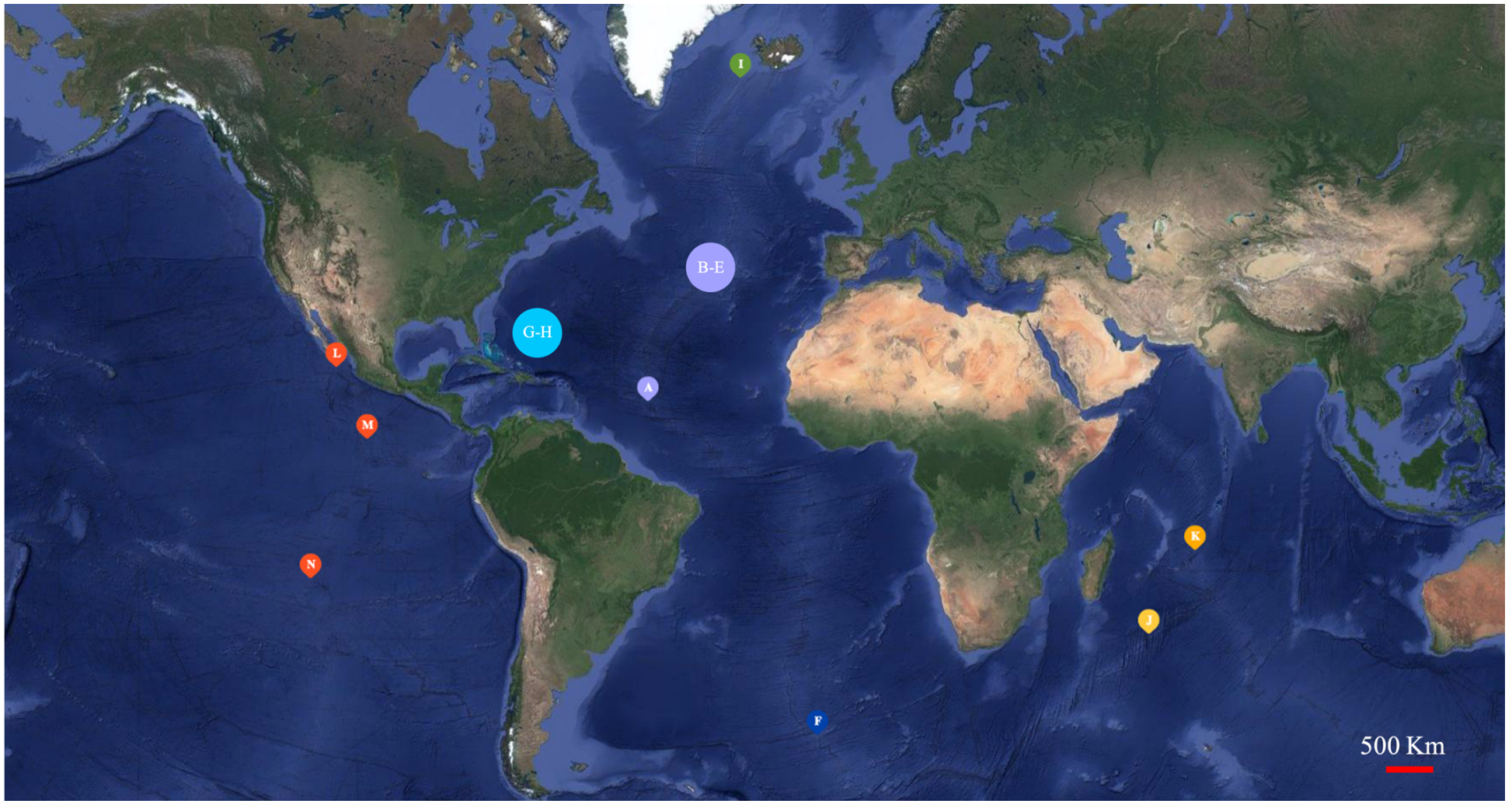


Figure 2: Geographical locations of the sampled MORB. Each letter corresponds to an individual sample (details are provided in Table 4). The samples are grouped by the ridges they were obtained from: lavender points (A, B, C, D, E) represent samples from the Northern Mid-Atlantic Ridge (NAR), deep blue point (F) is for the Southern Mid-Atlantic Ridge (SAR), light blue points (G, H) indicate Cretaceous MORB from the NAR, green point (I) is from the Reykjanes ridge, yellow point (J) is from the South-West Indian Ridge (SWIR), orange point (K) is from the Central Indian Ridge (CIR) and red points (L, M, N) are from the East-Pacific Rise (EPR). Samples B, C, D and E are in close proximity and marked by a single point, as are G and H. The geographical positions were obtained from the literature (She et al., 2023; Wood et al., 1979) and this map was created using the Mapize online tool, with satellite imagery provided by Google resources.

3. Analytical techniques

3.1. Laboratories, tools and reagents

The samples were processed in a class 100 clean room at the Institut de Physique du Globe de Paris (IPGP), France. For purification purposes, the acids (6 mol/L HCl, 16 mol/L HNO₃, and 27 mol/L HF) were obtained by sub-boiling distillation of commercial-grade reagents. Optima™ quality 8.8 mol/L HBr was purchased from Fischer Scientific.

3.2. Sample digestion

For most terrestrial igneous rocks, about 1 to 2 g of powdered sample were weighted and then digested using a mixture of 5 mL concentrated HNO₃ and 5 mL concentrated HF in a closed screw-cap Teflon vial. Biological samples (ERM BB 186) were digested in a mixture of concentrated HNO₃ and H₂O₂ in order to breakdown organic compounds. Vials were heated at 120°C on a box-type hotplate for 3 to 4 days, until complete digestion was achieved. The samples were then evaporated to dryness at 100°C, and refluxed in 10 to 20 mL of 6 mol/L HCl at 100°C for one week, until complete conversion of the residue into the chloride form was achieved. During this phase, the samples were regularly placed in an ultrasonic bath to facilitate fluorides breakdown. Spiking was performed when the samples were dissolved in HCl.

3.3. Double spiking

In this work, we utilized the DS method to correct for experimental and instrumental isotope fractionation. To ensure the quality of the data, the spike/sample ratio, defined as $\left(\frac{m_{Cd\ spike}}{m_{Cd\ sample} + m_{Cd\ spike}}\right)$, was kept as close as possible to the optimum ratio of 0.35 (Rudge et al., 2009). Therefore, knowledge of the sample Cd concentration was essential. Prior to spiking, a small aliquot of the solution was analyzed using an Agilent quadrupole ICP-MS at the IPGP facility, to determine the Cd concentration. We mixed the remaining sample with a ^{106}Cd - ^{111}Cd DS, characterized by a $^{106}Cd / ^{110}Cd$ isotopic ratio of 350 and a $^{111}Cd / ^{110}Cd$ ratio of 228, aiming at the optimal spike/sample ratio. After spiking, we refluxed the sample for 48h on a hotplate in order to ensure full sample-spike equilibration.

In order to assess the influence of the spike over sample ratio on the quality of the data, we analyzed a ChemLab pure Cd standard spiked with different amounts of DS. The table S1 and figure S1 synthesize the results of this experiment. We experimented with spike/sample ratios ranging from 0.14 (60 % deficit to the optimum) to 0.45 (30 % overabundance relative to the optimum ratio), which covers almost the entire range observed for our spiked samples (except for the two slightly overspiked komatiite samples SCH 1.9 and Welt 564-5 having spike/sample ratios of 0.48 and 0.50, respectively). No significant deviation from the reference value (see Table 3), nor significant change in the uncertainties, were observed within this range of spike/sample ratios.

3.4. Cadmium purification by anion exchange chromatography

Cadmium was separated from Sn and the sample matrix using a chemical protocol inspired by that used by [Schmitt et al. \(2009\)](#) for Cd separation and by established methods for Zn (Moynier and Le Borgne, 2015; Van Kooten and Moynier, 2019) and In (Liu et al., 2023) stable isotope measurements. This protocol uses an anion exchange, chloride form, resin (Bio-Rad

AG 1x8 200-400 mesh). The protocol requires five consecutive iterations of the purification of the Cd fraction to completely remove Sn, as detailed in Table 2. The first run was unique because it required the dissolution of a significant amount of sample. Therefore, a 1.5 mol/L HBr solution was used for the first run, while 0.1 mol/L HBr solutions were used for the four other runs. This did not impact the elution of Cd, as Cd's distribution coefficient with the anion exchange resin remains very high in both 1.5 mol/L or 0.1 mol/L HBr (see elution curves, calibrated on a BCR-2 basalt sample: Table S2, S3 and Figure S2). Based on our elution data, we retained only ~ 0.5 % of the initial Sn content after the first purification run. Then, with the second protocol (used from the second run to the fifth), we removed ~ 95 % of the Sn each time.

Thus, after the second purification run, only around 0.03 % of the initial Sn content remains, which becomes less than 0.01 % after the third run. After the fifth purification run, the initial Sn/Cd ratio should have been divided by a few thousands, while collecting 99.6 wt.% of the sample Cd. We then dried down the collected Cd solution cut on a hot plate, at 80°C, and refluxed it with concentrated nitric acid at 110°C for a day to destroy residual resin particles. Analytical Cd blanks ranged from 7 to 55 pg, with a median of 15 pg, representing less than 1 wt.% of the total Cd mass of the sample.

Table 2: Details of the Cd purification protocol

	Procedure step	Reagent	Volume (mL)
Every run	Resin introduction	AG 1x8 200-400mesh	0.2
	Resin cleaning	Mili-Q water	3
		0.5 M HNO ₃	3
		Mili-Q water	3
1 st run only	Conditioning	1.5 M HBr	3
	Sample load*	1.5 M HBr	5
	Matrix removing*	0.1 M HBr	5
Every run except 1st	Conditioning	0.1 M HBr	3
	Sample load	0.1 M HBr	2
Every run	Matrix removing	0.1 M HBr	12
	Cd elution	0.1 M HNO ₃	12

The table outlines the detailed procedure used to purify Cd and eliminate Sn from the matrix. In reagent column, M notation stands for mol/L. Samples were purified 5 times, with introduction and cleaning of the resin in the Teflon column being similar at every iteration. The first run for each sample differed from the other four runs as a more concentrated solution of HBr (1.5 mol/L) was used for the dissolution of the sample due to the high matrix content. *During the first run, the sample was

introduced 0.5mL at a time, followed by 0.5mL HBr 0.1 mol/L to remove matrix and prevent column clogging. The other four purifications did not require this precaution as most matrix had already been discarded and so the sample could be directly dissolved in HBr 0.1 mol/L.

3.5. Mass spectrometry and data reduction

Samples were analyzed either on a *ThermoFischer Neptune* or a *ThermoFischer Neptune Plus* multi-collector ICP-MS at the IPGP facility, equipped with nickel Jet and H skimmer cones. Sample introduction was carried out using an autosampler coupled to an ESI IR Apex desolvation system (hot sector at 120°C, cold sector at 2°C), with an uptake rate of 100 $\mu\text{L}/\text{min}$.

We monitored six cadmium isotopes, namely ^{106}Cd , ^{110}Cd , ^{111}Cd , ^{113}Cd , ^{114}Cd , and ^{116}Cd . However, due to potential major isobaric interferences from ^{116}Sn (14.3 molar % of the total Sn) on ^{116}Cd , only ^{106}Cd , ^{110}Cd , ^{111}Cd and ^{113}Cd or ^{114}Cd were used for deconvolution. There also may still be some interferences from Sn on mass 114, as ^{114}Sn makes up 0.6 molar % of the total Sn content. Indium interferences on ^{113}Cd were also corrected for. In order to evaluate and correct the intensity of interference from In and Sn isotopes, we also measured the ^{115}In and ^{118}Sn signals.

All measurements were conducted in 0.5 mol/L nitric acid, with Cd concentrations ranging from 10 to 25 ppb. Sample analyses were bracketed by spiked standard solutions to ensure accurate assessment of isotope variations. We usually attain sensitivities around 300 V/ppm on all cumulated Cd signals, or 80 V/ppm on ^{114}Cd . Individual data points were derived from a block of 50 individual measurements, roughly consuming 0.7 mL of the sample solution in 7 min. The precision attained in this work ranges from 0.01 to 0.03 ‰ per amu, which is similar to that of most recent studies (Pickard et al., 2022) (see Figure 1).

Some analyses were conducted to determine the influence of concentration mismatch over the $\delta^{114}\text{Cd}$ value. A standard AAS solution (AAS in the following) (Lot# 1797541), used in [Liu et al. \(2020\)](#), as well as the NIST SRM 2711 soil sample, were analyzed at different concentrations against a 25 ppb NIST 3108 standard. The AAS solution and NIST SRM 2711

concentrations were ranging from 15 (-40 %) to 36 ppb (+44 %) and 22 (-12 %) to 32 ppb (+28 %), respectively. Results are summarized in Table S4 and Figure S3. No significant deviation from the reference value was observed in any cases. The Cd isotope compositions always overlapped with their reference value. Thus, our analysis method is resilient over 40 % of standard/sample intensity mismatch. In any case, during the analysis, sample and standard Cd concentrations were matched to be within 10 % intensity.

To obtain accurate DS isotopic data, we performed a deconvolution step using the *IsoSpike* integration-by-integration algorithm (Creech and Paul, 2015). Uncertainties for most samples were determined by calculating the 2SD obtained for repeated analyses of the sample. When the samples were analyzed only once or twice during the session, we used the largest 2SD uncertainties obtained for another sample analyzed under the same conditions and during the same analytical session. The Cd concentrations were determined using the spike proportion given as an output by the algorithm.

3.6. Interference assessment and correction

Tin is the main cause for interferences on the Cd isotopes used for data deconvolution. In order to correct any potential remaining isobaric interferences, we used the abundance of ^{118}Sn and assumed natural isotopic ratios of $^{114}\text{Sn}/^{118}\text{Sn} = 0.02725$, $^{116}\text{Sn} / ^{118}\text{Sn} = 0.60033$ and $^{117}\text{Sn} / ^{118}\text{Sn} = 0.31709$ (Berglund and Wieser, 2011). To determine the limits of this approach, we carried out further experiments using Sn-doped double-spiked NIST SRM 3108 Cd standard solutions. We varied the Cd/Sn ratios from 4000 to 2.5, with a Cd concentration of 25 ppb. Figure S4 displays the results of these experiments, detailed in table S5. Uncorrected Sn interferences produced a significant bias in the measured $\delta^{114}\text{Cd}$ values larger than our analytical error ($0.087 \pm 0.06 \%$) when $\text{Cd}/\text{Sn} \leq 450$. After chemical purification, the Cd fraction has usually a Cd/Sn ratio > 500 , and, therefore, the Sn interference should have a negligible effect on the measured $\delta^{114}\text{Cd}$. In any case, the Sn interference was corrected for.

This correction is effective for Cd/Sn as low 4.5, which is higher than in any of our samples after the chemical purification.

To assess the effect of the isobaric interference of ^{113}In on ^{113}Cd , we followed a similar protocol to that described above for Sn and the results are displayed in table S5. The $\delta^{113}\text{Cd}$ value is affected even for relatively low In concentrations ($\text{Cd/In} < 16\,500$). However after chemical purification, most samples had Cd/In ratios over 20 000, and in any case, potential interferences were corrected for by using ^{115}In abundance and assuming a natural $^{113}\text{In} / ^{115}\text{In}$ ratio of 0.04482 (Berglund and Wieser, 2011). The correction algorithm is efficient for $\text{Cd/In} \geq 24$.

The effect of isobaric interferences from ^{106}Pd and ^{110}Pd were tested using a similar approach. Significant effects (larger than our analytical uncertainty) were detected on $\delta^{114}\text{Cd}$ for Cd/Pd ratio lower than 472 and on $\delta^{113}\text{Cd}$ for Cd/Pd ratio lower than ~ 4000 (see table S6). Isobaric interferences would create apparent mass-independent isotope compositions. All the data reported fall on a straight line of slope 4/3 in the $\delta^{114}\text{Cd}$ vs. $\delta^{113}\text{Cd}$ space, as expected for a mass-dependent fractionation, further demonstrating the absence or efficient correction for any isobaric interferences.

Finally, polyatomic isobaric interferences can also affect some Cd isotopes (May and Wiedmeyer, 1998), notably from Mo or Zr. Significant effects on the $\delta^{114}\text{Cd}$ values were found when Cd/Mo was lower than 5 and Cd/Zr lower than 264 (see table S6). However, all of our samples have Cd/Mo and Cd/Zr ratios higher than 1804 and 428 respectively. Therefore, no significant effects are expected from these two elements.

3.7. Analyzed SRM – determination of the method's validity

We present a comprehensive dataset of Cd isotopic composition and concentration measurements for 11 standard materials, including two standard solutions of Cd. Calibration of our analytical process was performed by analyzing two pure Cd ICP-MS standard solutions,

ChemLab (lot# CL01.0301.0100) and AAS (Lot# 1797541), against the NIST SRM 3108 Cd standard solution. The AAS standard solution was obtained from the University of Science and Technology of China (USTC), in Hefei. It was previously characterized to have a $\delta^{114}\text{Cd}$ of $-0.691 \pm 0.041 \text{ ‰}$ (Liu et al., 2020).

We analyzed seven well-characterized United States Geological Survey (USGS) Geological Reference Materials (GRM): AGV-2 (andesite, Guano Valley, Oregon, USA), BCR-2 (basalt, Columbia River, Oregon, USA), BHVO-2 (basalt, Kilauea, Hawaii, USA), BIR-1a (basalt, Reykjavik region, Iceland), COQ-1 (carbonatite, Canada), GSP-2 (granodiorite, Silver Plume, Colorado, USA) and NOD-A-1 (manganese nodule powder from the Atlantic Ocean floor), as well as one biostandard (ERM BB 186, dried and powdered pork kidney, Institute for Reference Materials and Measurements, Geel, Belgium) and a standard reference material from the USA, NIST SRM 2711 (polluted soil from Montana, USA) that were selected based on their high Cd concentrations and heavy isotope compositions (Borovička et al., 2021; Cloquet et al., 2005; Liu et al., 2020; Pallavicini et al., 2014). While only a few of these reference materials were well characterized for cadmium isotope compositions until recently (Cloquet et al., 2005; Horner et al., 2010; Li et al., 2018; Murphy et al., 2016; Pallavicini et al., 2014; Wombacher et al., 2003), recent progress in high precision Cd isotope analyses has renewed interests in such studies, resulting in the reporting of additional geostandard Cd isotope compositions (Borovička et al., 2021; Chang et al., 2023; Liu et al., 2020; Lu et al., 2021; Pickard et al., 2022; Tan et al., 2020). However, only one study (Liu et al., 2020) report the Cd isotopic composition for COQ-1, and GSP-2.

4. Results

The Table 3 displays the isotope compositions and Cd concentrations for the standard samples. All the discussed mean values, as well as results for Chemlab and AAS, are weighted means and standard deviations, defined as:

$$\text{weighted mean} = \delta_{mean} = \frac{\sum_i \delta_i \times w_i}{\sum_j w_j}$$

$$\text{and weighted 2SD} = 2 \times \sqrt{\frac{N \times \sum_i [w_i \times (\delta_i - \delta_{mean})^2]}{(N-1) \times \sum_j w_j}}$$

Where δ_i is the individual isotope composition measurement, w_i is the individual weight associated with this measurement and is defined as equal to $1/(2SD)$ and N is the number of separate isotope measurements taken into account in the calculation.

The ChemLab Cd standard and NIST 3108 Cd solution have similar isotopic compositions, with $\delta^{114}Cd_{chemlab} = 0.02 \pm 0.02 \text{ ‰}$. On the other hand, the AAS solution has a significantly distinct isotope composition, with $\delta^{114}Cd_{AAS} = -0.67 \pm 0.04 \text{ ‰}$. The USGS GRM AGV-2, BCR-2, BHVO-2, BIR-1a, COQ-1, GSP-2, and NOD-A-1 have less fractionated Cd isotope compositions, with $\delta^{114}Cd$ values ranging between $-0.03 \pm 0.07 \text{ ‰}$ (GSP-2) and $0.23 \pm 0.02 \text{ ‰}$ (COQ-1, 2SD, n = 3). In contrast, the polluted soil NIST SRM 2711 and biostandard ERM BB 186 exhibit heavier isotopic compositions: $\delta^{114}Cd_{NIST 2711} = 0.67 \pm 0.04 \text{ ‰}$ and $\delta^{114}Cd_{ERM BB 186} = 0.60 \pm 0.07 \text{ ‰}$ (2SD, n = 2). Most SRM typically have Cd concentrations of a few hundred ppb. However, some standards, such as NOD-A-1, NIST 2711, COQ-1, and ERM-BB-186, are highly enriched in Cd, with concentrations as high as 37 ppm.

Basaltic samples collected from mid-oceanic ridges generally exhibit homogeneous Cd isotope compositions and concentrations (Table 4 and Figure 4). Regardless of their origin, their isotopic compositions fall within the range of $0.01 \pm 0.10 \text{ ‰}$ to $0.13 \pm 0.10 \text{ ‰}$, overlapping within uncertainties. Cadmium concentrations in these samples range from 91 to 151 ppb. Only

one sample (DSDP 51A 417A) shows significantly different characteristics. This sample is enriched in Cd and is isotopically light, with 386 ppb and $\delta^{114}\text{Cd}_{\text{DSDP 51A 417A}} = -0.42 \pm 0.04 \text{ ‰}$ (compared with the 138 ppb and $\delta^{114}\text{Cd}_{\text{DSDP 52 417D}} = 0.09 \pm 0.08 \text{ ‰}$, for the other Cretaceous Atlantic sample).

The Cd isotope compositions of komatiites exhibit much greater variability than those of MORB, ranging from -0.33 ± 0.04 to $0.26 \pm 0.08 \text{ ‰}$ (see Table 5). They have low Cd concentrations, ranging from 27 to 92 ppb. Neither isotope compositions nor concentrations are correlated with locality. Most samples (except two) are isotopically similar or heavier than the mean MORB composition.

Table 3: Cd isotope compositions and concentration of standard reference materials

Sample	Description	Location	Spike proportion	$\delta^{113}\text{Cd}$ (‰)	2SD	n	$\delta^{114}\text{Cd}$ (‰)	2SD	n	References	Cd (ppb)	2SD	References
AAS	Reference solution		0.33	-0.51	0.03	121	-0.67	0.04	124	This study			
							-0.69	0.04	57	Liu et al. (2020)			
Chemlab	Reference solution		0.37	0.03	0.03	200	0.02	0.02	202	This study			
AGV-2	Andesite	Guano Valley, OR., USA	0.35	0.15	0.02	10	0.22	0.03	10		69		
			0.34	0.15	0.06	7	0.20	0.05	7		72		
Mean	weighted			0.15	0.01	2	0.21	0.04	2	This study	71	4	This study
											66	4	Du and Hu (2015)
											58	4	Xu et al. (2015)
											69		Braukmüller et al. (2020)**
							0.09	0.04	8	Liu et al. (2020)	70		Liu et al. (2020)**
							0.14	0.05	3	Pickard et al. (2022)	68		Pickard et al. (2022)**
BCR-2	Basalt	Columbia River, OR., USA	0.37	0.06	0.10	10	0.08	0.12	10		206		
			0.35	0.08	0.04	9	0.09	0.08	9		215		
			0.35	0.08	0.02	10	0.11	0.04	10		198		
Mean	weighted			0.07	0.01	3	0.10	0.02	3	This study	206	17	This study
											155	13	Du and Hu (2015)
											148	7	Xu et al. (2015)
											204		Braukmüller et al. (2020)**
							0.02	0.07	14	Liu et al. (2020)	209		Liu et al. (2020)**
							-0.03	0.06	4	Tan et al. (2020)	220		Tan et al.(2020)**
							0.01	0.07	6	Lu et al. (2021)	180		Lu et al. (2021)**
							0.01	0.04	4	Pickard et al. (2022)	207		Pickard et al. (2022)**
							-0.02	0.04	3	Chang et al. (2023)	180		Chang et al. (2023)**

Table 3 (continued)

Sample	Description	Location	Spike proportion	$\delta^{113}\text{Cd}$ (‰)	2SD	n	$\delta^{114}\text{Cd}$ (‰)	2SD	n	References	Cd (ppb)	2SD	References
BHVO-2	Basalt	Kilauea, Hawaii, USA	0.34	0.10	0.04	11	0.15	0.03	11	This study	92		This study
											107	8	Du and Hu (2015)
											93		Wang et al. (2015)**
											95		Braukmüller et al. (2020)**
											88	8	Liu et al. (2020)**
											200	4	Tan et al. (2020)**
											90	6	Lu et al. (2021)**
											88	6	Pickard et al. (2022)**
	86	42	Chang et al. (2023)**										
BIR-1a	Basalt	Iceland	0.36	0.14	0.07	10	0.22	0.07	10		94		
			0.39	0.12	0.01	5	0.15	0.02	5	*	78		
Mean	weighted		0.12	0.02	2	0.17	0.09	2	This study	86	22	This study	
			0.14	0.52	6	Wombacher et al. (2003)							
			93	8	Du and Hu (2015)								
			96		Braukmüller et al. (2020)**								
			98	12	Liu et al. (2020)**								
	93	4	Pickard et al. (2022)**										
COQ-1	Carbonatite	Canada	0.36	0.17	0.03	19	0.24	0.02	19		613		
			0.41	0.17	0.06	17	0.22	0.01	18	*	450		
			0.42	0.19	0.06	11	0.24	0.02	11	*	455		
Mean	weighted		0.17	0.02	3	0.23	0.02	3	This study	506	185	This study	
										556	42	Du and Hu (2015)	
			0.10	0.05	8	Liu et al. (2020)	600		Liu et al. (2020)**				

Table 3 (continued)

Sample	Description	Location	Spike proportion	$\delta^{113}\text{Cd}$ (‰)	2SD	n	$\delta^{114}\text{Cd}$ (‰)	2SD	n	References	Cd (ppb)	2SD	References		
ERM BB 186	Pork Kidney		0.37	0.44	0.07	5	0.60	0.07	5	This study	979		This study		
										Pallavicini et al. (2014)			1040	100	Pallavicini et al. (2014)
										Borovicka et al. (2021)					
GSP-2	Granodiorite	Silver Plume, CO., USA	0.36	-0.05	0.03	5	-0.03	0.07	5	This study	88		This study		
													106	8	Du and Hu (2015)
										Liu et al. (2020)			91		Liu et al. (2020)**
NIST SRM 2711	Montana soil	Montana, USA	0.37	0.50	0.01	10	0.67	0.04	10	This study	37363		This study		
										Cloquet et al. (2005)					
										Pallavicini et al. (2014)			41700		Pallavicini et al. (2014)
										Liu et al. (2020)					
NOD-A-1	Manganese nodule	Atlantic Ocean	0.36	0.18	0.08	10	0.23	0.04	10		7141				
			0.37	0.17	0.06	30	0.22	0.06	30		6914				
Mean	weighted			0.17	0.01	2	0.22	0.02	2	This study	7027	322	This study		
							-0.05	0.23	1	Cloquet et al. (2005)	7500		Cloquet et al. (2005)		
							0.23	0.08	2	Horner et al. (2010)	6810		Horner et al. (2010)		
							0.09	0.03	4	Pallavicini et al. (2014)	7280	620	Pallavicini et al. (2014)		
							0.17	0.05	6	Murphy et al. (2016)					
							0.16	0.10	4	Li et al. (2018)	7500		Li et al. (2018)**		
							0.12	0.07	14	Tan et al. (2020)	6130		Tan et al. (2020)**		
							0.12	0.01	5	Borovicka et al. (2021)					
							0.13	0.04	7	Lu et al. (2021)					
							0.13	0.03	15	Chang et al. (2023)	6170		Chang et al. (2023)**		

Separate rows indicate multiple digestions of the sample. n : number of mass spectrometer runs for a given digestion or number of independent digestions (for mean values). 2SD uncertainties for the Cd concentrations were calculated if multiples independent digestions of the same sample were available. Sample with * in the "References" field were spiked before HNO₃-HF digestion

*to check for potential isotope fractionation during digestion. Literature concentrations with ** after the article reference were determined by isotope dilution. (Borovička et al., 2021; Braukmüller et al., 2020; Chang et al., 2023; Cloquet et al., 2005; Du and Hu, 2015; Horner et al., 2010; Li et al., 2018; Liu et al., 2020; Lu et al., 2021; Murphy et al., 2016; Pallavicini et al., 2014; Pickard et al., 2022; Tan et al., 2020; Wang et al., 2015; Wombacher et al., 2003; Xu et al., 2015)*

Table 4: Characterization of studied MORB

Sample	Corresponding letter on Figure 1	age (Ma)	Location	Spike proportion	$\delta^{113}\text{Cd}$ (‰)	2SD	n	$\delta^{114}\text{Cd}$ (‰)	2SD	n	References	Cd (ppb)
Atlantic Ocean												
2 π D 44-1	A	0	North Atlantic Ridge (NAR)	0.279	0.04	0.04	10	0.07	0.03	10	This study	110
ARP 74 7 8 surface	B	0	North Atlantic Ridge (NAR)	0.246	-0.01	0.07	11	0.01	0.10	11	This study	151
ARP 74 9 13 C	C	0	North Atlantic Ridge (NAR)	0.293	0.03	0.01	13	0.06	0.02	13	This study	148
CH31 DR12 137	D	0	North Atlantic Ridge (NAR)	0.26	0.04	0.06	7	0.09	0.09	7	This study	101
CH30 DR17-03	E	0	North Atlantic Ridge (NAR)	0.281	0.08	0.03	8	0.13	0.10	8	This study	91
ERW 9309 2D-1g	F	0	South Atlantic Ridge (SAR)	0.372	0.01	0.06	3	0.01	0.05	3	This study	117
DSDP 51A-417A	G	109	Carbonaceous Atlantic Sample (CAS)	0.357	-0.34	0.01	8	-0.42	0.04	9	This study	386
DSDP 52-417D	H	109	Carbonaceous Atlantic Sample (CAS)	0.246	0.03	0.08	10	0.09	0.08	10	This study	138
DSDP LEG 49 409	I	2.3	Reykjanes Ridge	0.21	0.02	0.09	9	0.05	0.12	9	This study	133
Mean Atlantic Ocean MORB	weighted				0.03	0.05	8	0.06	0.07	8	This study	
POS 221 604 DS-1G			S.Kolbeinsey Ridge					0.12	0.09	2	Pickard et al. (2022)	152
M41/2 130 DS-3			Southern Mid Atlantic Ridge					0.02	0.04	2	Pickard et al. (2022)	71
M41/2 142 DS-2			Southern Mid Atlantic Ridge					0.07	0.05	2	Pickard et al. (2022)	115

Table 4 (continued)

Sample	Corresponding letter on Figure 1	age (Ma)	Location	Spike proportion	$\delta^{113}\text{Cd}$ (‰)	2SD	n	$\delta^{114}\text{Cd}$ (‰)	2SD	n	References	Cd (ppb)
A127 DR15			Azores Plateau					0.12	0.04	1	Pickard et al. (2022)	118
Mean Atlantic Ocean MORB	weighted							0.06	0.08	12	This study and Pickard et al. (2022)	
Indian Ocean												
MD34 D1	J	0	South West Indian Ridge (SWIR)	0.344	0.06	0.04	11	0.10	0.04	11	This study	133
MD57 D6-7	K	0	Central Indian Ridge (CIR)	0.231	0.09	0.01	7	0.11	0.04	7	This study	94
Mean Indian Ocean MORB	weighted				0.07	0.04	2	0.10	0.02	2	This study	
MD57 D10-1			Indian Ocean					0.24	0.05	1	Pickard et al. (2022)	132
Mean Indian Ocean MORB	weighted							0.14	0.13	3	This study and Pickard et al. (2022)	
Pacific Ocean												
CYP 78 12-34	L	0	East-Pacific Rise (EPR)	0.268	0.01	0.10	11	0.04	0.08	11	This study	130
Sea Rise 1 DR04 301	M	0	East-Pacific Rise (EPR)	0.272	0.02	0.07	11	0.04	0.08	11	This study	139

Table 4 (continued)

Sample	Corresponding letter on Figure 1	age (Ma)	Location	Spike proportion	$\delta^{113}\text{Cd}$ (‰)	2SD	n	$\delta^{114}\text{Cd}$ (‰)	2SD	n	References	Cd (ppb)
Sea Rise 2 DR03	N	0	East-Pacific Rise (EPR)	0.259	0.04	0.03	8	0.06	0.07	8	This study	121
Mean Pacific Ocean MORB	weighted				0.02	0.03	3	0.05	0.02	3	This study	
MW 87/2 87-6			East Pacific Rise					0.12	0.07	2	Pickard et al. (2022)	160
SO157 54 DS-1			Pacific Antarctic Rise					0.08	0.05	3	Pickard et al. (2022)	152
SO157 63 DS-1			Pacific Antarctic Rise					0.07	0.05	4	Pickard et al. (2022)	302
SO80 37 DS-1			Pukao Seamount					0.06	0.04	2	Pickard et al. (2022)	133
SO80 43 DS-1			Pukao Seamount					0.00	0.05	2	Pickard et al. (2022)	132
Mean Pacific Ocean MORB	weighted							0.06	0.08	8	This study and Pickard et al. (2022)	
Mean MORB	weighted							0.07	0.10	23	This study and Pickard et al. (2022)	

Ages and geographical positions are taken from Emmermann and Puchelt (1980), She et al. (2023), and Wood et al. (1979). Published data (in grey) are from Pickard et al. (2022).

Table 5: Description and isotope compositions of komatiites

Sample	Description	Locality	Region	age (Ma)	2SD	Loss on ignition (LOI) (wt.%)	Spike proportion	$\delta^{113}\text{Cd}$ (‰)	2SD	n	$\delta^{114}\text{Cd}$ (‰)	2SD	n	References	Cd (ppb)	References
BC 02	Px spinifex	Boston Creek	Abitibi greenstone belt. Canada	2720	2	3.0	0.23	0.16	0.09	3	0.26	0.08	3	This study	87	This study
BC 03	Px spinifex	Boston Creek	Abitibi greenstone belt. Canada	2720	2	1.6	0.23	0.12	0.09	4	0.18	0.08	3	This study	89	This study
Kost 9497	Ol spinifex	Kostomuksha	Baltic shield	2843	39	5.2	0.26	0.07	0.07	5	0.12	0.03	2	This study	74	This study
Kost 94123	Ol spinifex	Kostomuksha	Baltic shield	2843	39	6.1	0.36	-0.04	0.06	6	-0.04	0.05	2	This study	68	This study
PH 27	Ol spinifex	Pyke Hill	Abitibi greenstone belt. Canada	2713	29	6.7	0.33	0.14	0.06	8	0.20	0.05	2	This study	44	This study
PH 28	Ol spinifex	Pyke Hill	Abitibi greenstone belt. Canada	2713	29	6.1	0.31	0.01	0.09	9	0.08	0.08	1	This study	60	This study
SCH 1.1	Ol spinifex	Schapenburg	Barberton greenstone belt. South Africa	3549	99	4.2	0.30	0.14	0.09	10	0.23	0.08	3	This study	66	This study
SCH 1.5	Ol spinifex	Schapenburg	Barberton greenstone belt. South Africa	3549	99	2.8	0.26	0.00	0.03	11	0.02	0.04	5	This study	92	This study
SCH 1.9	Ol cumulate	Schapenburg	Barberton greenstone belt. South Africa	3549	99	7.1	0.48	0.07	0.08	12	0.08	0.05	1	This study	34	This study
Welt 12-2	Ol spinifex	Weltevereden	Barberton greenstone belt. South Africa	3266	8	8.1	0.26	-0.14	0.08	15	-0.19	0.09	3	This study	77	This study
Welt 564-4	Ol spinifex	Weltevereden	Barberton greenstone belt. South Africa	3266	8	7.9	0.22	0.11	0.08	16	0.14	0.05	1	This study	50	This study

Table 5 (continued)

Sample	Description	Locality	Region	age (Ma)	2SD	Loss on ignition (LOI) (wt.%)	Spike proportion	$\delta^{113}\text{Cd}$ (‰)	2SD	n	$\delta^{114}\text{Cd}$ (‰)	2SD	n	References	Cd (ppb)	References
Welt 564-5	Ol spinifex	Weltevereden	Barberton greenstone belt. South Africa	3266	8	8.4	0.50	0.05	0.08	17	0.10	0.08	2	This study	27	This study
MT 20	Ol spinifex	Munro Township	Abitibi greenstone belt. Canada	2714	2	7.9					-0.33	0.04	3		47	
M657	Ol spinifex	Alexo Mine	Abitibi greenstone belt. Canada	2690	15	6					0.12	0.03	2	Pickard et al. (2022)	48	Pickard et al. (2022)
KAL-1	Ol spinifex	Alexo Mine	Abitibi greenstone belt. Canada	2690	15	7.3					-0.12	0.1	1			
ZA-1	Ol spinifex	Belingwe	Belingwe greenstone belt. Zimbabwe	2690	13	3.37					0.03	0.05	2		77	

Pristine komatiites **weighted** **LOI < 6 wt. %** **0.14** **0.18** **5** **This study and Pickard et al. (2022)**

Sample descriptions, locations, ages and LOI values are from existing literature (Byerly et al., 2017; Chauvel et al., 1993; Connolly et al., 2011; Corfu and Noble, 1992; Dupré et al., 1984; Lahaye and Arndt, 1996; Nisbet et al., 1987; Puchtel et al., 2018, 2016, 2013, 2009, 2004, 1998; Puchtel and Humayun, 2005; Rehkämper et al., 1999). Additional samples (in grey) from Munro Township, Alexo Mine (Abitibi greenstone belt, Canada) and Belingwe (Belingwe greenstone belt, Zimbabwe) are from Pickard et al. (2022). Ol stands for olivine, Px for pyroxene.

5. Discussion

5.1. Standard samples – validation of the method

Two standard solutions, ChemLab Cd solution and AAS, were used in this study. AAS had previously been analyzed to have a $\delta^{114}\text{Cd}$ of $-0.69 \pm 0.04 \text{ ‰}$ (Liu et al., 2020), which is consistent with the value of $-0.67 \pm 0.04 \text{ ‰}$ obtained in this study (see Table 3). Since AAS is a pure Cd solution, it was only spiked, diluted and analyzed, without being processed through the Cd purification protocol. Therefore, this result can only be used to ensure the correct calibration and the efficiency of the double spike system and that no problem occurs during analysis. With this agreement between our data and literature, we concluded that our ^{106}Cd - ^{111}Cd double spike system was calibrated satisfactorily and that the analysis protocol produced correct results.

Several studies have reported Cd concentration data for the standard samples analyzed here (Braukmüller et al., 2020; Chang et al., 2023; Cloquet et al., 2005; Du and Hu, 2015; Horner et al., 2010; Li et al., 2018; Liu et al., 2020; Lu et al., 2021; Pallavicini et al., 2014; Pickard et al., 2022; Tan et al., 2020; Wang et al., 2015; Xu et al., 2015). Our measured Cd concentrations are consistent with these values, except for NIST 2711 for which we have a 10 % deficit compared to the published value (Pallavicini et al., 2014). For some samples (BIR-1a and COQ-1), the uncertainties (2SD) on our Cd concentrations are respectively 25 and 35 %. Some of these samples were spiked following digestion, and it is possible that some Cd was lost by evaporation prior to spiking. However, even if this is the case, the similarity of the isotope compositions of the samples spiked before or after digestion show that this process would not have significantly affected its isotopic composition. Alternatively, these differences in concentration could also represent heterogenous distribution of Cd between different lots of the reference standards.

Most of our samples have a $\delta^{114}\text{Cd}$ that overlaps with at least one of the previously reported values (Borovička et al., 2021; Chang et al., 2023; Cloquet et al., 2005; Horner et al., 2010; Li et al., 2018; Liu et al., 2020; Lu et al., 2021; Murphy et al., 2016; Pallavicini et al., 2014; Pickard et al., 2022; Tan et al., 2020; Wombacher et al., 2003), although they are generally on the heavier side of the previous estimates (see Figure 3). For three samples, COQ-1, ERM BB 186 and GSP-2, our $\delta^{114}\text{Cd}$ is about 0.1 ‰ higher (Borovička et al., 2021; Liu et al., 2020; Pallavicini et al., 2014). It should be noted that there was only one previous measurement for COQ-1 and GSP-2 and two for ERM BB 186.

Given that the spiked AAS solution was analyzed at the same time as these samples and returned a similar $\delta^{114}\text{Cd}$ value to that obtained at USTC (Liu et al., 2020), it can be concluded that the DS calibration, the mass-spectrometry and the deconvolution step are not the source of potential shifts. We also tested whether Cd isotopes could have been fractionated prior to adding the double spike, i.e., at the sample dissolution stage. However, replicates of BIR-1a and COQ-1 that were double-spiked before or after digestion returned similar $\delta^{114}\text{Cd}$ values (see Table 3). This implies that no isotopic fractionation occurs at the digestion stage, as was previously also suggested (Vlastelic and Piro, 2022). Finally, as demonstrated above, we have tested that all reported data have $\delta^{114}\text{Cd}$ and $\delta^{113}\text{Cd}$ values that follow mass-dependency, refuting the presence of noticeable isobaric interferences. Moreover, all the MORB samples (except for the anomalous DSDP 51A-417A, which is discussed later) have isotope compositions that are consistent with that from the literature ($[0.01 \pm 0.05; 0.13 \pm 0.10 \text{ ‰}]$ in this work, versus $[0.00 \pm 0.05; 0.24 \pm 0.05 \text{ ‰}]$ in Pickard et al. (2022)). These MORB samples, as well as the AAS solution, were analyzed along with the geo- and biostandards. Standard samples can potentially be affected by contamination due to their large-scale production, as previously demonstrated based on isotopically heterogeneous Mo between different batches (Willbold et al., 2016; Willbold and Elliott, 2017). It is, therefore, possible

that some of the Cd isotopic variability observed here is due to contamination during processing; however, it has not been demonstrated that Cd was present in the grinding equipment used for the production of such samples. In any case, we consider that our results are representative of the isotope compositions of the samples.

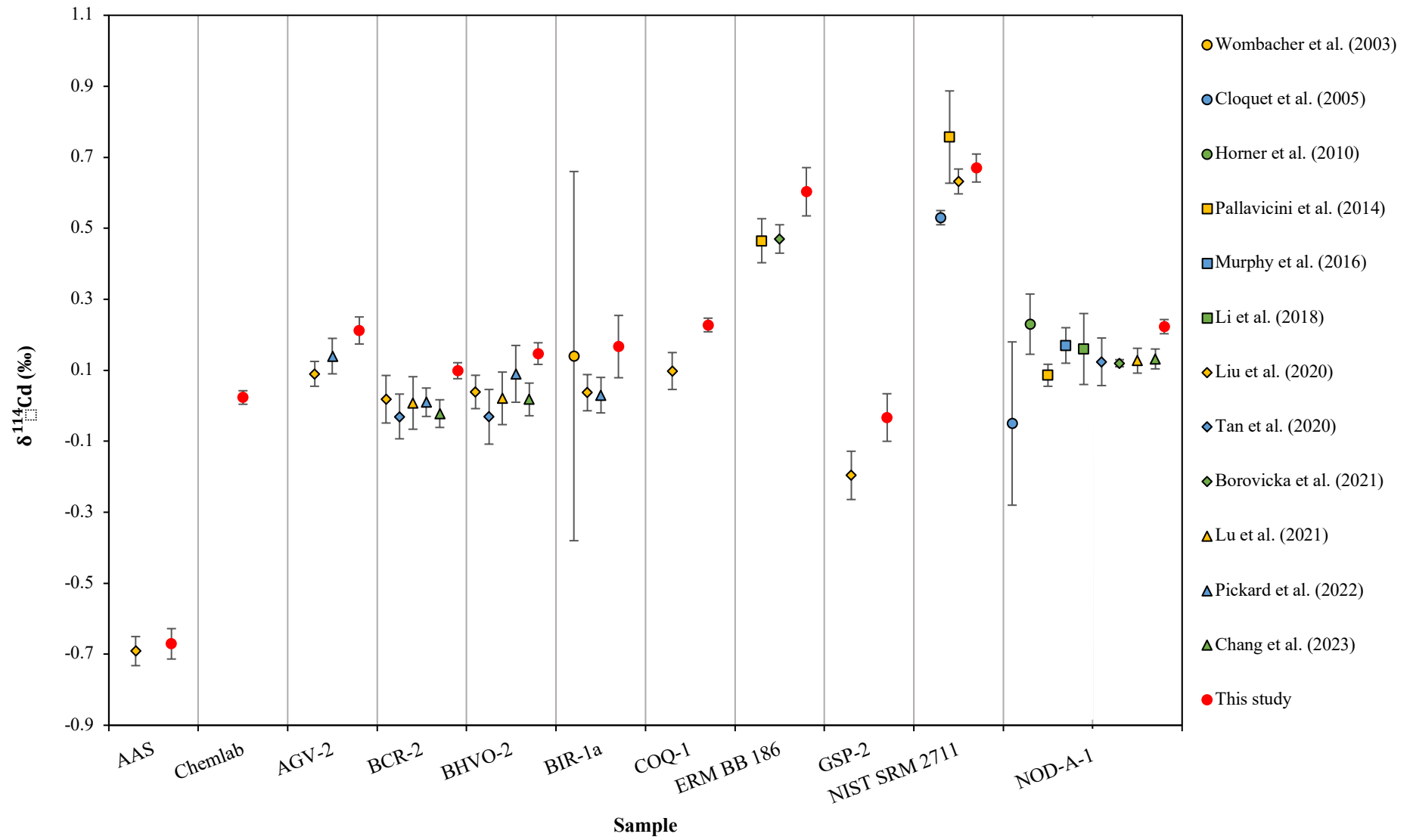


Figure 3: Isotope compositions of geological and biological standard reference materials, compared with the literature data. Red circles correspond to the weighted values obtained in this study; the corresponding error bars represent weighted 2SD. Our results generally overlap with at least some estimations from the literature. However, in many cases it is at the isotopically heavier end of the previously proposed values. Since AAS pure Cd solution does not present such characteristic, we can assess that it does not reflect instrumental bias. All these samples have isotope compositions that fall on the 4/3 sloped mass dependency line in a $\delta^{114}\text{Cd}$ vs. $\delta^{113}\text{Cd}$ space, indicating that no interference is at play here. Such shift could result from geostandard contamination during processing. Sources of the data: (Borovička et al., 2021; Chang et al., 2023; Cloquet et al., 2005; Horner et al., 2010; Li et al., 2018; Liu et al., 2020; Lu et al., 2021; Murphy et al., 2016; Pallavicini et al., 2014; Pickard et al., 2022; Tan et al., 2020; Wombacher et al., 2003))

5.2. The mid-oceanic ridge basalts

The Cd concentration of MORB are homogeneous across the literature, regardless of their locality of origin, giving a mean Cd concentration of 119 ± 45 ppb (2SD, $n = 31$) (Yi et al., 2000), 129 ± 53 ppb (2SD, $n = 9$) (Pickard et al., 2022) or 124 ± 39 ppb (2SD, $n = 13$) (this work). This homogeneity indicates that Cd volatilization, which has been shown to be significant for sub-aerial basalts (Yi et al., 2000), is probably negligible for submarine MORB.

The Cd isotopic compositions of MORB also exhibit remarkable homogeneity both within and between the ridges (Figure 4). Our data show excellent agreement with those from the literature (Pickard et al., 2022). However, one outlier that stands out is sample DSDP 51A 417A. This outlier is one of the two Cretaceous basalts sampled from the Caribbean Sea, it has higher Cd concentration and is isotopically lighter than any other MORB. Previous studies (Emmermann and Puchelt, 1980; She et al., 2023) have described it as being more altered than DSDP 52 417D and also representing a unique Sn isotope composition among MORB. Exposure to seawater may have led to the enrichment of light Cd isotopes by Cd adsorption (Peng et al., 2023; Wasylenki et al., 2014), precipitation of calcite containing isotopically light Cd (Horner et al., 2011), although no anomalous amount of CaO was measured by She et al. (2023), crystallization of isotopically light CdS sulfides (Guinoiseau et al., 2018; Xie et al., 2019) or by another, still unrecognized, mechanism. Each mechanism would contribute to the

observed light Cd isotope composition by adding isotopically light Cd to the sample. Given this probable input, we consider DSDP 51A 417A to be non-representative of MORB and have excluded it from further discussion.

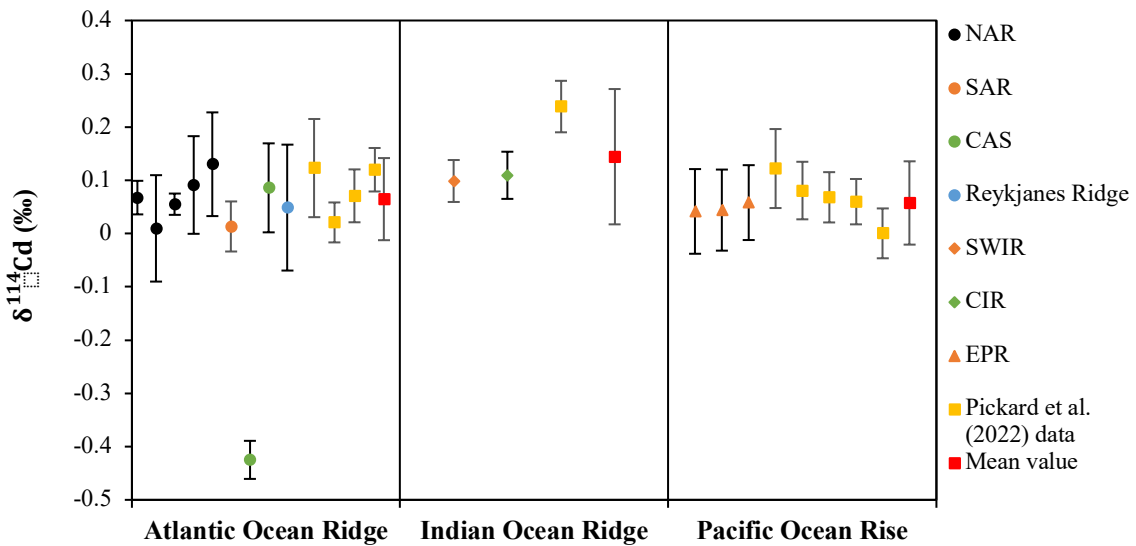


Figure 4: Isotope composition of MORB, arranged by locality. The localities include NAR: North Atlantic ridge, SAR: South Atlantic ridge, CAS: Cretaceous Atlantic sample, SWIR: South West Indian ridge, CIR: central Indian ridge, EPR: East Pacific rise. The error bars represent 2 weighted standard deviations. The mean isotope composition for each ocean is calculated using both our data and the literature data, with the exception of the isotopically fractionated CAS data point, which is discarded. Isotope compositions of the MORB samples are remarkably similar regardless of the ridge they originated from. This observation led us to propose that the depleted MORB mantle is isotopically homogeneous for Cd. Additional details are provided in Table 4.

To compare the Cd isotopic compositions of MORB between different ridge systems, mean values were calculated for each system. This was done first with our own data, literature data (Pickard et al., 2022), and finally with a combination of our own and literature data Pickard et al. (2022). For the Atlantic Ocean, the weighted mean isotope composition calculated using our data (0.06 ± 0.07 ‰, 2SD, $n = 8$), is similar to the literature weighted mean composition of 0.08 ± 0.10 ‰ (2SD, $n = 4$) and to the combined value of 0.06 ± 0.08 ‰ (2SD, $n = 12$). Similarly, for the Pacific Ocean, our data (0.05 ± 0.02 ‰, 2SD, $n = 3$) are in good agreement

with the literature data ($0.06 \pm 0.08 \text{ ‰}$, 2SD, $n=5$), resulting in a total weighted mean Cd isotope composition of $0.06 \pm 0.08 \text{ ‰}$ (2SD, $n = 8$).

For the Indian Ocean, the isotope compositions of the three samples are more variable than in the other oceans. Thus, the weighted mean isotope composition of MORB from the Indian Ocean was calculated to be $0.10 \pm 0.02 \text{ ‰}$ (2SD, $n = 2$) for our samples and $0.14 \pm 0.13 \text{ ‰}$ (2SD, $n = 3$) when the MORB data from the literature are included. The weighted mean Cd isotope composition of each of the three oceanic systems significantly overlaps, with a mean MORB Cd isotope composition of $0.07 \pm 0.10 \text{ ‰}$ (2SD, $n = 23$).

The Cd isotopic compositions of the MORB samples are remarkably consistent regardless of ages and locations. This suggests that, although processes such as variable degrees of partial melting, fractionated crystallization or volatilization may have affected the final Cd abundance of the different MORB samples, they did not generate significant Cd isotope variations within the currently achievable precision.

5.3. Ocean island basalts

Unlike MORB, OIB samples from the literature (Pickard et al., 2022; Schmitt et al., 2009a; Yi et al., 2000) are characterized by very diverse Cd concentrations, ranging from 43 to 324 ppb, and diverse isotope compositions, ranging from $-0.10 \pm 0.05 \text{ ‰}$ to $0.50 \pm 0.05 \text{ ‰}$ (see Figure 5). These variations could reflect chemical heterogeneities in their mantle sources (caused by input of subducted material or primordial mantle heterogeneities), and/or igneous processes, such as variations in the degree of melting, volatilization, and fractional crystallization.

The Cd depletion, reported specifically for sub-aerial lavas (Pickard et al., 2022; Schmitt et al., 2009a; Yi et al., 2000), seems to confirm that significant Cd volatilization can occur for lavas erupted sub-aerially. This volatilization could produce significant isotope fractionation

even with relatively small Cd loss (Wombacher et al., 2004), with the residue drifting toward Cd-depleted and isotopically heavy compositions.

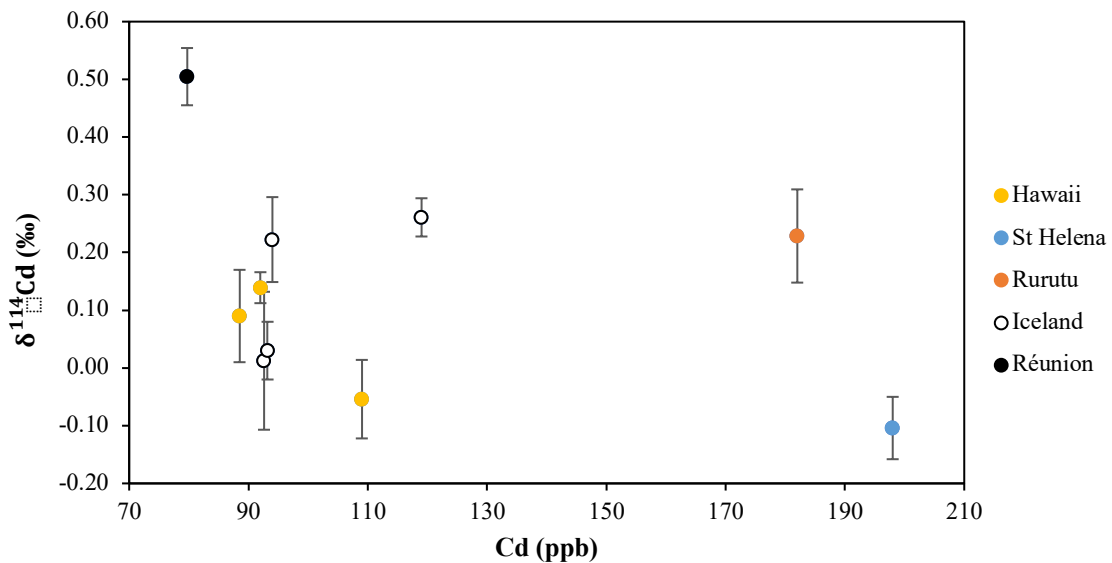


Figure 5: OIB compositions from five localities. No obvious correlation is visible that could indicate the main fractionating process. Isotope compositions could result from a mix of volatilization, light Cd isotopes input and alteration. It is also possible that some of these compositions are inheritors of isotopically fractionated specific mantle domains. (Pickard et al., 2022; Schmitt et al., 2009; This study)

Secondary processes, such as seawater alteration, could also alter the OIB isotope compositions. Studies have shown that alteration is a Cd-depleting process and that residues drift toward light isotope compositions (Zhang et al., 2016; Zhu et al., 2018). Thus, it could explain the depleted and light compositions observed for some OIBs from Hawaii and Iceland. Given that specific compositions could also be inherited from mantle source or by addition of subducted material, the interpretation of the OIB data is more complex than those for MORBs or komatiites.

5.4. Cadmium in komatiites: alteration and the Archean mantle signature

In contrast to the consistent isotopic compositions of the MORB samples, the isotopic compositions of komatiites are variable. One of the main differences that may explain such variability is their degree of alteration. Other processes that could produce such variable isotope

compositions would be Cd volatilization before cooling of the lava or other secondary processes, such as metamorphism or metasomatism.

Isotope fractionation through Cd volatilization is expected to produce a correlation between the Cd concentration and the isotope composition of the sample. Specifically, we expect Cd-rich samples to be isotopically lighter than the most depleted ones, which is not observed. To the contrary, the most Cd-rich samples are also among the isotopically heaviest. Thus, volatilization does not seem to explain the variability of komatiites Cd compositions. Similarly, metamorphism or metasomatism cannot be the cause for such variability, as we would expect processes like these to produce significant isotope variations between samples from different localities, which is not the case, as similar heavy isotope compositions are found in the samples from every locality.

Alteration has most probably affected the komatiites significantly. Samples located near the top of the lava flows have been exposed to seawater upon and after emplacement; this process may have affected the highly mobile Cd. Specifically, hydrothermal fluids may have preferentially leached out the heavy Cd isotopes, leading to lighter isotopic composition in the remaining residue (Zhang et al., 2016; Zhu et al., 2018).

We consider the loss on ignition (LOI) (Sueoka et al., 1985), which represents the amount of volatile species (primarily water and CO₂) in the sample, as an indicator of the degree of alteration. CO₂ constitutes only a small percentage of the LOI when it is under ~12 % (Cortiade et al., 2022; Tamblyn et al., 2023); thus LOI is considered a useful measure of hydration, for igneous rocks, particularly basalts (Arel and Tugrul, 2001; Irfan, 1999; Tugrul and Gurbinar, 1997). It has also been used as a proxy for the serpentinization rate (Cortiade et al., 2022; Mayhew and Ellison, 2020; Tamblyn et al., 2023; Zhou et al., 2022). The studied komatiites underwent different degrees of serpentinization, which is reflected in the LOI values ranging from 1.6 to 8.4 wt. %.

There is a correlation between LOI and Cd concentrations, with a clear linear negative trend observed across all samples from our dataset and the literature, except for one noticeable outlier (Welt 12-2) (see Figure 6 (a)). This trend is consistent with our understanding of Cd mobility in hydrothermal fluids, where leaching can result in Cd loss. It also shows that alteration is the main process affecting Cd concentrations in komatiites.

The outlier, Welt 12-2, has a Cd content that is approximately double that of other samples with similar LOI values. One explanation for this anomaly would be that its LOI value is artificially higher due to significant CO₂ amounts that were fixed in the sample by calcite precipitation. This would typically result in a higher CaO content, which is not observed (Puchtel et al., 2013). This suggests that the LOI value reflects hydration rather than carbonation, and that the outlier is due to anomalously high Cd content. It is possible that the sample was enriched in Cd after lava emplacement, via the previously discussed mechanisms (Guinoiseau et al., 2018; Wasylenki et al., 2014; Xie et al., 2019).

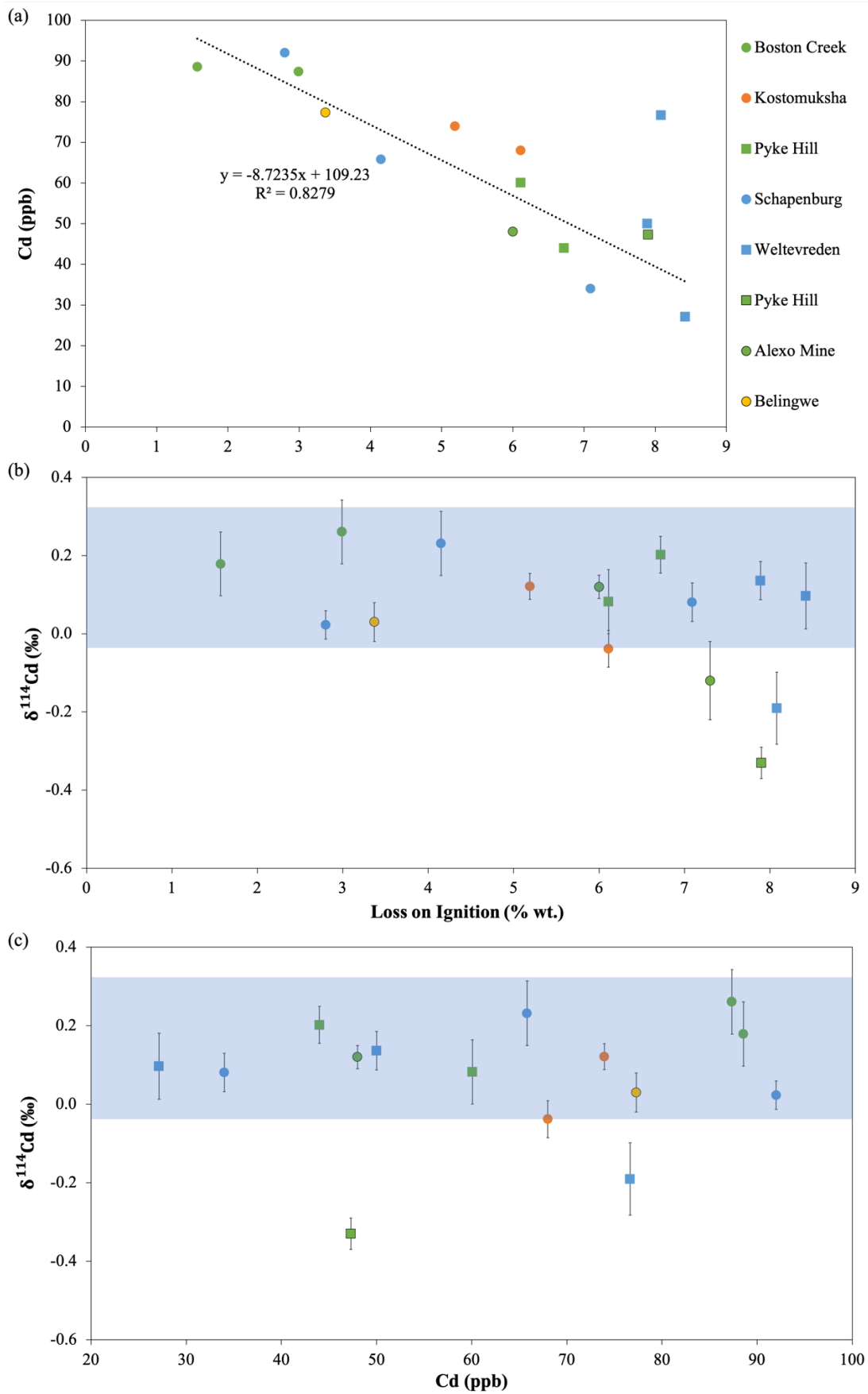


Figure 6: Cadmium contents (a) and isotope compositions (b) of the komatiites plotted as a function of the Loss on Ignition (LOI). Panel (c) represents Cd isotope compositions of komatiites plotted as a function of their Cd content. Green circles and squares correspond to samples from the Abitibi Greenstone Belt (AGB), Canada, blue ones correspond to samples from the Barberton Greenstone Belt (BGB), South Africa, orange circles refer to samples from the Baltic Shield and yellow circle to sample from the Belingwe Greenstone Belt, Zimbabwe. Shapes with black rims refer to data from the literature (Pickard et al., 2022). (a) The Cd content follows a negative linear correlation with LOI, regardless of locality or age, except for one sample from Weltevreden and one from Schapenburg which are significantly enriched in Cd compared to other samples with similar LOI. (b) Although the non-anomalous komatiites are distributed along the LOI axis, their isotope compositions are very similar and often overlap, indicating that komatiite isotope compositions are quite resilient to alteration. The blue band embodies the mean isotope composition of the pristine komatiites (LOI < 6 wt. %).

The observed Cd depletion could result in significant isotope fractionation in the remaining komatiites, as heavy Cd isotopes loss can occur during alteration (Zhang et al., 2016; Zhu et al., 2018). Figure 6 (b) and (c), respectively, display isotope compositions of komatiites plotted as a function of their LOI and their Cd content. Although the heaviest compositions are similar regardless of LOI, there seems to be a trend toward lighter isotope enrichment when LOI is high and Cd content low, suggesting isotope fractionation during alteration.

In order to determine a reference isotope composition for pristine komatiites, we need to focus our analysis on the least altered samples. We will thereafter only consider samples below an arbitrary LOI threshold of 6 wt.%. Such value allows us to select only the least altered samples while having at least one komatiite from every geological region in our dataset. The isotope compositions of these samples are generally heavy, with two isotopically lighter outliers: SCH 1.5 and ZA-1. The previously mentioned outlier samples Welt 12-2 and SCH 1.5 present similarities, as both samples are enriched in Cd and are isotopically lighter than samples from the same location. This is contrary to what is expected from the general trend, in which Cd-rich samples are isotopically heavy. We propose that these samples have experienced a significant input of light isotopes of Cd from an unknown source. Furthermore, since their Cd contents and isotope compositions do not seem to be linked to the LOI (the Schapenburg

sample having low LOI when the Weltevreden one has high LOI), we assess that the enriching process is not coupled with hydration. Thus, SCH 1.5 is regarded as unrepresentative and not taken into account for determination of a pristine komatiites Cd isotope composition. We obtained a weighted mean isotope composition for pristine komatiites of $\delta^{114}\text{Cd}_{\text{pristine komatiites}} = 0.14 \pm 0.18 \text{ ‰}$ (2SD, $n = 5$). This value is undistinguishable from the mean Cd isotope composition of MORB.

The ages of analyzed komatiite range from $3549 \pm 99 \text{ Ma}$ for Schapenburg (Puchtel et al., 2009) to $2690 \pm 15 \text{ Ma}$ (Dupré et al., 1984) and $2690 \pm 13 \text{ Ma}$ (Chauvel et al., 1993) for Alexo and Belingwe, respectively (see Figure 7). Despite this large spread in age, pristine komatiite samples from different locations show identical isotope compositions. This suggests that the isotope composition of the Archean deep mantle likely remained largely constant $0.14 \pm 0.18 \text{ ‰}$ (2SD, $n = 5$), and that this homogenization process occurred before the formation of the Schapenburg komatiites, at least $3549 \pm 99 \text{ Ma}$ ago. This conclusion, however, does not negate the potential existence of local Cd isotope heterogeneities.

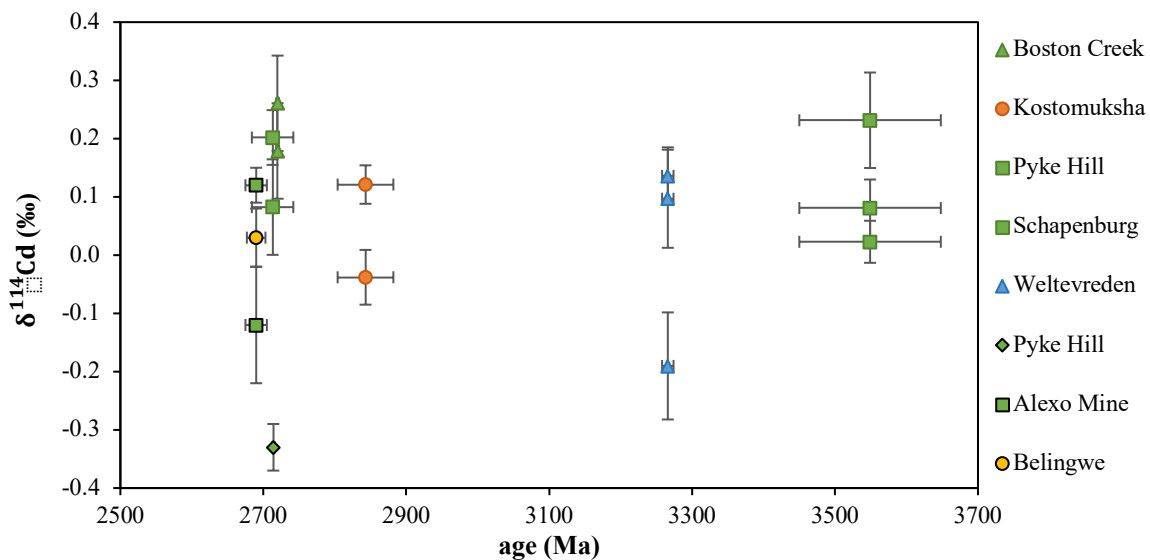


Figure 7: Cadmium isotope compositions of komatiites plotted against their individual ages. Green symbols represent samples from the Abitibi Greenstone Belt (AGB), Canada, blue ones correspond to samples from the Barberton Greenstone Belt (BGB), South Africa, orange circles refer to samples from the Baltic Shield and yellow circle to one sample from the Belingwe

Greenstone Belt, Zimbabwe. Markers with black rims represent data from the literature (Pickard et al., 2022). Despite being separated in time by almost one billion years, the isotope compositions of the BGB and AGB are similar. This suggests that the Cd isotope composition was homogeneous in the Archean mantle and that this homogeneity was established at least 3.5 billion years ago.

5.5. Comparison between the literature estimations

A previous study (Pickard et al., 2022) estimated that pristine komatiites are isotopically lighter than both MORB and OIB. Moreover, most of the peridotites analyzed in Pickard et al. (2022) are isotopically lighter than MORB and OIB but closer to some komatiitic compositions. The authors proposed a BSE isotope composition of -0.06 ± 0.03 ‰ (2SD, n = 4), based on the data for spinel lherzolites. Additionally, these conclusions suggest that magmas produced by the lower degrees of partial melting (e.g., OIB) are isotopically heavier than their mantle sources. This peridotite-based estimation is in agreement with the only other proposed BSE isotope composition for Cd, of -0.04 ± 0.02 ‰ (2SD, n = 7), which is based on analysis of loesses, MORB and OIB (Schmitt et al., 2009a).

Although the obtained BSE compositions are similar, comparison between the data sets does generate problems. Indeed, even if individual data points from both studies do overlap significantly, most MORB, OIB and loess samples from Pickard et al. (2022) are isotopically heavier than the BSE composition proposed by Schmitt et al. (2009), even though it is based on similar samples. If we apply Schmitt et al. (2009) approach (a mean of loesses, OIB and MORB compositions) to the larger dataset of Pickard et al. (2022), we obtain a BSE composition of 0.11 ± 0.14 ‰ (2SD, n = 28), which is significantly heavier than what was proposed by Pickard et al. (2022). Thus, it seems that both methods for BSE characterization (via peridotites or via igneous rocks) actually diverge.

Peridotite-based Cd isotope compositions for the BSE should be the most robust, as peridotites represent direct sampling from the mantle. However, peridotite xenoliths have been

affected by partial melting and secondary processes that could have caused significant isotope fractionation (Zhang et al., 2016; Zhu et al., 2018).

5.6. The effects of partial melting

We concluded that komatiites and MORB share similar Cd isotope compositions, indicating that the isotope fractionation of Cd occurring during partial melting is negligible for MORB and for samples formed by higher degrees of partial melting (komatiites). Thus, the compositions of these samples should reflect that of their mantle sources. On the other hand, OIB compositions are too scattered and potentially too affected by isotopic fractionation processes (partial melting, Cd volatilization and/or secondary processes) to propose a reliable isotope composition for their mantle source. Therefore, we propose that:

$$\delta^{114}\text{Cd}_{\text{DMM}} = \delta^{114}\text{Cd}_{\text{MORB}} = 0.07 \pm 0.10 \text{ ‰} \text{ (2SD, } n = 23\text{)}$$

$$\delta^{114}\text{Cd}_{\text{Archean mantle}} = \delta^{114}\text{Cd}_{\text{pristine komatiites}} = 0.14 \pm 0.18 \text{ ‰} \text{ (2SD, } n = 5\text{)}$$

These isotope compositions are much heavier than what was proposed for spinel lherzolites ($-0.06 \pm 0.03 \text{ ‰}$, 2SD, $n = 4$) (Pickard et al., 2022). This would be consistent with a significant loss of heavy Cd isotopes in these peridotites, possibly by alteration processes. In the absence of pristine peridotites or undegassed OIB isotope compositions, we cannot characterize the isotope fractionation occurring during low degrees of partial melting. Determination of Cd isotope compositions for submarine OIB that did not experience significant Cd loss by volatilization might be the way to resolve this problem.

5.7. Determination of the Cd isotope composition of the Earth's mantle

The Cd isotope composition of the mantle can be represented by a combination of isotope compositions of MORB and komatiites. However, since our sample set is dominated by MORB, calculating a mean value for all 28 samples would artificially skew the mantle isotope composition towards MORB value. To address this, we have chosen to consider the mantle

isotope composition as equally accounted for by the DMM and the Archean mantle, giving the following formula:

$$\delta^{114}\text{Cd}_{\text{mantle}} = \frac{\delta^{114}\text{Cd}_{\text{DMM}} + \delta^{114}\text{Cd}_{\text{Archean mantle}}}{2} = 0.11 \pm 0.10 \text{ ‰ (2SD, n = 28)}$$

The fact that the isotope compositions of the DMM and Archean mantle, determined independently, are similar provides strong support for the conclusion that the mantle is significantly isotopically heavier than was proposed in the previous studies (Pickard et al., 2022; Schmitt et al., 2009a), as shown on Figure 8.

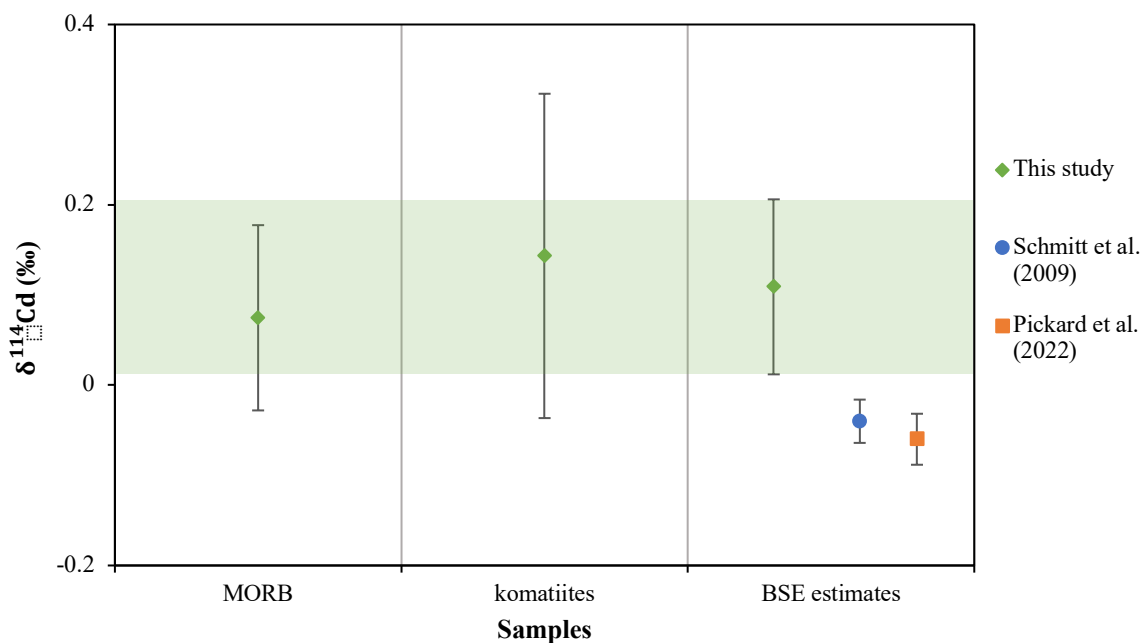


Figure 8: Comparison of the proposed Cd isotope composition of the mantle with the literature values and isotope compositions of different rock types. The green field represents the preferred proposed isotope composition for the mantle (based on the data for MORB and komatiites). There is no overlap with the previous isotope compositions proposed for the mantle (Pickard et al., 2022; Schmitt et al., 2009a).

5.8. From the mantle to the Bulk Earth

To assess the influence of the mantle on the Cd isotope composition of the Bulk Earth (BE), we need to estimate the distribution of Cd in the different reservoirs. The mass of the BE, including those of the mantle, core, and crust, are respectively estimated to be 5.9736×10^{24} Kg, 4.043×10^{24} Kg, 1.932×10^{24} Kg and 2.6×10^{22} Kg (Yoder, 1995). Thus, the BSE represents 68

wt.% of the BE. It is estimated that the continental crust constitutes 0.57 wt.% of the mantle mass (Rudnick, 1995), which amounts to 2.30×10^{22} Kg. This estimate leaves 2.95×10^{21} Kg for the oceanic crust.

Cadmium concentration of the BE has been determined to be 80 ± 20.8 ppb (Wang et al., 2018). The same study proposed that the core has a Cd concentration of 167 ± 63 ppb, while the BSE has a Cd concentration of 38.3 ± 5.6 ppb. The continental crust has a Cd concentration of 80 ppb (Rudnick and Gao, 2014). Here we propose a mean Cd concentration of 126 ± 45 ppb for the oceanic crust, based on the data for MORB glasses. Based on these data, the BE contains 4.78×10^{17} Kg of Cd, with 1.56×10^{17} Kg Cd in the BSE and 3.23×10^{17} Kg Cd in the core (67.5 wt.% of the total Cd content), consistent with Cd being both chalcophile and siderophile. As was seen previously, the rest of the Cd budget is dominated by the mantle.

The core's high Cd concentration makes it the most important reservoir to consider when studying the BE composition. Any isotopic variation between the core and the mantle would have a significant impact on the overall BE isotopic composition. Recent work suggests that Cd is unlikely to undergo any significant isotope fractionation during the formation of the Earth's core (Pickard et al., 2023). Therefore, the core and mantle should have similar Cd isotopic composition, leading to the following BE isotope composition:

$$\delta^{114}\text{Cd}_{BE} = \delta^{114}\text{Cd}_{BSE} = 0.11 \pm 0.10 \text{ ‰ (2SD, n = 28)}$$

6. Conclusions

This study determined the Cd isotope compositions of a large set of terrestrial rocks to provide a new estimate of $\delta^{114}\text{Cd}_{BSE}$. The Cd isotope compositions of 9 available rocky and biological standards were characterized using a ^{106}Cd - ^{111}Cd double spike method, and the new data showed general agreement with the previous results. The isotope composition of the MORB samples indicated a remarkable isotopic homogeneity within an individual ridge, as

well as a great similarity between different ridges, with a proposed mean $\delta^{114}\text{Cd}_{\text{MORB}}$ of $0.07 \pm 0.10 \text{ ‰}$ (2SD, $n = 23$). The mean isotope composition for pristine komatiites shows a value of $0.14 \pm 0.18 \text{ ‰}$ (2SD, $n = 5$), and indicates that the Archean mantle has had a homogeneous Cd isotope composition since at least $3549 \pm 99 \text{ Ma}$ ago. By coupling these results, the study defined a new value for $\delta^{114}\text{Cd}_{\text{BSE}}$ of $0.11 \pm 0.10 \text{ ‰}$ (2SD, $n = 28$) that can also be used to approximate the bulk Earth Cd isotope composition.

Acknowledgements:

We thank Fang Huang for providing the USTC AAS internal Cd standard. We thank Dimitri Rigoussen, Pascale Louvat, Marine Paquet and Tu-Han Luu for their help with chemical preparation of samples and mass-spectrometry. The manuscript greatly benefited from comprehensive and constructive reviews by Frank Wombacher and two anonymous reviewers and from editorial handling by Sonja Aulbach. This work was supported by the ERC grant agreement No. 101001282 (METAL) (F.M.).

7. References

Abouchami, W., Galer, S.J.G., de Baar, H.J.W., Middag, R., Vance, D., Zhao, Y., Klunder, M., Mezger, K., Feldmann, H., Andreae, M.O., 2014. Biogeochemical cycling of cadmium isotopes in the southern ocean along the zero meridian. *Geochim. Cosmochim. Acta* 127, 348–367. <https://doi.org/10.1016/j.gca.2013.10.022>

Abouchami, W., Galer, S.J.G., Horner, T.J., Rehkämper, M., Wombacher, F., Xue, Z., Lambelet, M., Gault-Ringold, M., Stirling, C.H., Schönbacher, M., Shiel, A.E., Weis, D., Holdship, P.F., 2013. A common reference material for cadmium isotope studies - NIST SRM 3108. *Geostand. Geoanalytical Res.* 37, 5–17. <https://doi.org/10.1111/j.1751-908X.2012.00175.x>

Arel, E., Tugrul, A., 2001. Weathering and its relation to geomechanical properties of Cavusbasi granitic rocks in northwestern Turkey. *Bull. Eng. Geol. Environ.* 60, 123–133. <https://doi.org/10.1007/s100640000091>

Aston, F.W., 1935. The isotopic constitution and atomic weights of hafnium, thorium, rhodium, titanium, zirconium, calcium, gallium, silver, carbon, nickel, cadmium, iron and indium. *Proc. R. Soc. Lond. Ser. - Math. Phys. Sci.* 149, 396–405. <https://doi.org/10.1098/rspa.1935.0070>

Aston, F.W., 1934. Mass-spectra and Isotopes. *J. Phys. Chem.* 38, 713–713. <https://doi.org/10.1021/j150356a016>

Badullovich, N., Moynier, F., Creech, J., Teng, F.-Z., Sossi, P.A., 2017. Tin isotopic fractionation during igneous differentiation and Earth's mantle composition. *Geochem. Perspect. Lett.* 5, 24–28. <https://doi.org/10.7185/geochemlet.1741>

Berglund, M., Wieser, M.E., 2011. Isotopic compositions of the elements 2009 (IUPAC Technical Report). *Pure Appl. Chem.* 83, 397–410. <https://doi.org/10.1351/PAC-REP-10-06-02>

Beunon, H., Mattielli, N., Doucet, L.S., Moine, B., Debret, B., 2020. Mantle heterogeneity through Zn systematics in oceanic basalts: Evidence for a deep carbon cycling. *Earth-Sci. Rev.* 205, 103174. <https://doi.org/10.1016/j.earscirev.2020.103174>

Böhlke, J.K., de Laeter, J.R., De Bièvre, P., Hidaka, H., Peiser, H.S., Rosman, K.J.R., Taylor, P.D.P., 2005. Isotopic compositions of the elements, 2001. *J. Phys. Chem. Ref. Data* 34, 57–67. <https://doi.org/10.1063/1.1836764>

Borovička, J., Ackerman, L., Rejšek, J., 2021. Cadmium isotopic composition of biogenic certified reference materials determined by thermal ionization mass spectrometry with double spike correction. *Talanta* 221, 121389. <https://doi.org/10.1016/j.talanta.2020.121389>

Braukmüller, N., Wombacher, F., Bragagni, A., Münker, C., 2020. Determination of Cu, Zn, Ga, Ag, Cd, In, Sn and Tl in geological reference materials and chondrites by isotope dilution ICP-MS. *Geostand. Geoanalytical Res.* 44, 733–752. <https://doi.org/10.1111/ggr.12352>

Braukmüller, N., Wombacher, F., Funk, C., Münker, C., 2019. Earth's volatile element depletion pattern inherited from a carbonaceous chondrite-like source. *Nat. Geosci.* 12, 564–568. <https://doi.org/10.1038/s41561-019-0375-x>

Byerly, B.L., Kareem, K., Bao, H., Byerly, G.R., 2017. Early Earth mantle heterogeneity revealed by light oxygen isotopes of Archaean komatiites. *Nat. Geosci.* 10, 871–875. <https://doi.org/10.1038/ngeo3054>

Chang, H., Zhu, J.-M., Wang, X., Gao, T., 2023. High-precision measurement of Cd isotopes in ultra-trace Cd samples using double spike-standard addition MC-ICP-MS. *J. Anal. At. Spectrom.* 38, 950–962. <https://doi.org/10.1039/D3JA00047H>

Chauvel, C., Dupré, B., Arndt, N.T., 1993. Pb and Nd isotopic correlation in Belingwe komatiites and basalts, in: Bickle, M.J., Nisbet, E.G. (Eds.), *The Geology of the Belingwe Greenstone Belt, Zimbabwe: A Study of the Evolution of Archaean Continental Crust*. CRC Press, p. 8. <https://doi.org/10.1201/9781003077596>

Cloquet, C., Carignan, J., Libourel, G., Sterckeman, T., Perdrix, E., 2006. Tracing source pollution in soils using cadmium and lead isotopes. *Environ. Sci. Technol.* 40, 2525–2530. <https://doi.org/10.1021/es052232+>

Cloquet, C., Rouxel, O., Carignan, J., Libourel, G., 2005. Natural cadmium isotopic variations in eight geological reference materials (NIST SRM 2711, BCR 176, GSS-1, GXR-1, GXR-2, GSD-12, Nod-P-1, Nod-A-1) and anthropogenic samples, measured by MC-ICP-MS. *Geostand. Geoanalytical Res.* 29, 95–106. <https://doi.org/10.1111/j.1751-908X.2005.tb00658.x>

Connolly, B.D., Puchtel, I.S., Walker, R.J., Arevalo, R., Piccoli, P.M., Byerly, G., Robin-Popieul, C., Arndt, N., 2011. Highly siderophile element systematics of the 3.3Ga Weltevreden komatiites, South Africa: Implications for early Earth history. *Earth Planet. Sci. Lett.* 311, 253–263. <https://doi.org/10.1016/j.epsl.2011.09.039>

Conway, T.M., John, S.G., 2015. Biogeochemical cycling of cadmium isotopes along a high-resolution section through the North Atlantic Ocean. *Geochim. Cosmochim. Acta* 148, 269–283. <https://doi.org/10.1016/j.gca.2014.09.032>

Corfu, F., Noble, S.R., 1992. Genesis of the southern Abitibi greenstone belt, Superior Province, Canada: Evidence from zircon Hf isotope analyses using a single filament technique. *Geochim. Cosmochim. Acta* 56, 2081–2097. [https://doi.org/10.1016/0016-7037\(92\)90331-C](https://doi.org/10.1016/0016-7037(92)90331-C)

Cortiade, N., Delacour, A., Guillaume, D., Moine, B., Chevet, J., 2022. Serpentinization of mantle xenoliths in Kerguelen archipelago: A first petrographic and geochemical study. *Lithos* 428–429, 106796. <https://doi.org/10.1016/j.lithos.2022.106796>

Creech, J.B., Paul, B., 2015. IsoSpike: improved double-spike inversion software. *Geostand. Geoanalytical Res.* 39, 7–15. <https://doi.org/10.1111/j.1751-908X.2014.00276.x>

Day, J.M.D., Moynier, F., Ishizuka, O., 2022. A partial melting control on the Zn isotope composition of basalts. *Geochem. Perspect. Lett.* 23, 11–16.

<https://doi.org/10.7185/geochemlet.2230>

Druce, M., Stirling, C.H., Bostock, H.C., Rolison, J.M., 2022a. Examining the effects of chemical cleaning, leaching, and partial dissolution on zinc and cadmium isotope fractionation in marine carbonates. *Chem. Geol.* 592, 120738.

<https://doi.org/10.1016/j.chemgeo.2022.120738>

Druce, M., Stirling, C.H., Bostock, H.C., Rolison, J.M., 2022b. Cadmium isotope systematics in sedimentary carbonate: Extending the utility of the cadmium isotope palaeo-productivity proxy. *Geochim. Cosmochim. Acta* 339, 80–96. <https://doi.org/10.1016/j.gca.2022.10.041>

Du, C., Hu, S., 2015. Accurate determination of trace cadmium in geological reference materials by closed vessel acid digestion ETAAS. *At. Spectrosc.* 36, 141–145. <https://doi.org/10.46770/AS.2015.03.005>

Dupré, B., Chauvel, C., Arndt, N.T., 1984. Pb and Nd isotopic study of two archean komatiitic flows from Alexo, Ontario. *Geochim. Cosmochim. Acta* 48, 1965–1972. [https://doi.org/10.1016/0016-7037\(84\)90378-8](https://doi.org/10.1016/0016-7037(84)90378-8)

Emmermann, R., Puchelt, H., 1980. Major and trace element chemistry of basalts from holes 417D and 418A, deep sea drilling project legs 51-53, in: Powell, R., Laughter, F. (Eds.), *Initial Reports of the Deep Sea Drilling Project, 51/52/53*. U.S. Government Printing Office, pp. 987–1000.

Guinoiseau, D., Galer, S.J.G., Abouchami, W., 2018. Effect of cadmium sulphide precipitation on the partitioning of Cd isotopes: Implications for the oceanic Cd cycle. *Earth Planet. Sci. Lett.* 498, 300–308. <https://doi.org/10.1016/j.epsl.2018.06.039>

Helffrich, G.R., Wood, B.J., 2001. The Earth's mantle. *Nature* 412, 501–507. <https://doi.org/10.1038/35087500>

Herzberg, C., 1992. Depth and degree of melting of komatiites. *J. Geophys. Res.* 97, 4521–4540. <https://doi.org/10.1029/91JB03066>

- Hirschmann, M.M., Stolper, E.M., 1996. A possible role for garnet pyroxenite in the origin of the “garnet signature” in MORB. *Contrib. Mineral. Petrol.* 124, 185–208. <https://doi.org/10.1007/s004100050184>
- Hofmann, A.W., 1997. Mantle geochemistry: the message from oceanic volcanism. *Nature* 385, 219–229. <https://doi.org/10.1038/385219a0>
- Horner, T.J., Rickaby, R.E.M., Henderson, G.M., 2011. Isotopic fractionation of cadmium into calcite. *Earth Planet. Sci. Lett.* 312, 243–253. <https://doi.org/10.1016/j.epsl.2011.10.004>
- Horner, T.J., Schönbacher, M., Rehkämper, M., Nielsen, S.G., Williams, H., Halliday, A.N., Xue, Z., Hein, J.R., 2010. Ferromanganese crusts as archives of deep water Cd isotope compositions: DATA BRIEF. *Geochem. Geophys. Geosystems* 11, n/a-n/a. <https://doi.org/10.1029/2009GC002987>
- Huang, J., Chen, S., Zhang, X., Huang, F., 2018. Effects of Melt Percolation on Zn Isotope Heterogeneity in the Mantle: Constraints From Peridotite Massifs in Ivrea-Verbano Zone, Italian Alps. *J. Geophys. Res. Solid Earth* 123, 2706–2722. <https://doi.org/10.1002/2017JB015287>
- Huppert, H.E., Stephen, R., Sparks, J., 1985. Cooling and contamination of mafic and ultramafic magmas during ascent through continental crust. *Earth Planet. Sci. Lett.* 74, 371–386. [https://doi.org/10.1016/S0012-821X\(85\)80009-1](https://doi.org/10.1016/S0012-821X(85)80009-1)
- Inglis, E.C., Moynier, F., Creech, J., Deng, Z., Day, J.M.D., Teng, F.-Z., Bizzarro, M., Jackson, M., Savage, P., 2019. Isotopic fractionation of zirconium during magmatic differentiation and the stable isotope composition of the silicate Earth. *Geochim. Cosmochim. Acta* 250, 311–323. <https://doi.org/10.1016/j.gca.2019.02.010>
- Irfan, T.Y., 1999. Characterization of weathered volcanic rocks in Hong Kong. *Q. J. Eng. Geol. Hydrogeol.* 32, 317–348.
- Kiseeva, E.S., Wood, B.J., 2013. A simple model for chalcophile element partitioning between

sulphide and silicate liquids with geochemical applications. *Earth Planet. Sci. Lett.* 383, 68–81. <https://doi.org/10.1016/j.epsl.2013.09.034>

Kubik, E., Siebert, J., Blanchard, I., Agranier, A., Mahan, B., Moynier, F., 2021. Earth's volatile accretion as told by Cd, Bi, Sb and Tl core–mantle distribution. *Geochim. Cosmochim. Acta* 306, 263–280. <https://doi.org/10.1016/j.gca.2021.02.017>

Lahaye, Y., Arndt, N., 1996. Alteration of a komatiite flow from Alexo, Ontario, Canada. *J. Petrol.* 37, 1261–1284. <https://doi.org/10.1093/petrology/37.6.1261>

Lambart, S., Koornneef, J.M., Millet, M.-A., Davies, G.R., Cook, M., Lissenberg, C.J., 2019. Highly heterogeneous depleted mantle recorded in the lower oceanic crust. *Nat. Geosci.* 12, 482–486. <https://doi.org/10.1038/s41561-019-0368-9>

Li, D., Li, M.-L., Liu, W.-R., Qin, Z.-Z., Liu, S.-A., 2018. Cadmium isotope ratios of standard solutions and geological reference materials measured by MC-ICP-MS. *Geostand. Geoanalytical Res.* 42, 593–605. <https://doi.org/10.1111/ggr.12236>

Liu, D., Moynier, F., Siebert, J., Sossi, P.A., Hu, Y., Kubik, E., 2022. Origin of moderately volatile element depletion on differentiated bodies: Insights from the evaporation of indium from silicate melts. *Geochim. Cosmochim. Acta* 339, 46–57. <https://doi.org/10.1016/j.gca.2022.09.043>

Liu, D., Moynier, F., Sossi, P.A., Pik, R., Halldórsson, S.A., Inglis, E., Day, J.M.D., Siebert, J., 2023. The indium isotopic composition of the bulk silicate Earth. *Geochim. Cosmochim. Acta* 352, 24–35. <https://doi.org/10.1016/j.gca.2023.04.018>

Liu, M., Zhang, Q., Zhang, Y., Zhang, Z., Huang, F., Yu, H., 2020. High-precision Cd isotope measurements of soil and rock reference materials by MC-ICP-MS with double spike correction. *Geostand. Geoanalytical Res.* 44, 169–182. <https://doi.org/10.1111/ggr.12291>

Loss, R.D., Rosman, K.J.R., De Laeter, J.R., 1984. Mass spectrometric isotope dilution analyses of palladium, silver, cadmium and tellurium in carbonaceous chondrites. *Geochim.*

- Cosmochim. Acta 48, 1677–1681. [https://doi.org/10.1016/0016-7037\(84\)90336-3](https://doi.org/10.1016/0016-7037(84)90336-3)
- Lu, Z., Zhu, J., Tan, D., Wang, X., Zheng, Z., 2021. $\delta^{114/110}$ Cd values of a suite of different reference materials. Geostand. Geoanalytical Res. 45, 565–581. <https://doi.org/10.1111/ggr.12380>
- Luck, J.-M., Othman, D.B., Albarède, F., 2005. Zn and Cu isotopic variations in chondrites and iron meteorites: Early solar nebula reservoirs and parent-body processes. Geochim. Cosmochim. Acta 69, 5351–5363. <https://doi.org/10.1016/j.gca.2005.06.018>
- Luck, J.M., Othman, D.B., Barrat, J.A., Albarède, F., 2003. Coupled ^{63}Cu and ^{16}O excesses in chondrites. Geochim. Cosmochim. Acta 67, 143–151. [https://doi.org/10.1016/S0016-7037\(02\)01038-4](https://doi.org/10.1016/S0016-7037(02)01038-4)
- Mahan, B., Siebert, J., Pringle, E.A., Moynier, F., 2017. Elemental partitioning and isotopic fractionation of Zn between metal and silicate and geochemical estimation of the S content of the Earth's core. Geochim. Cosmochim. Acta 196, 252–270. <https://doi.org/10.1016/j.gca.2016.09.013>
- Marin, N., Righter, K., Danielson, L., Pando, K., Lee, C., 2013. Metal-silicate partitioning of Bi, In, and Cd as a function of temperature and melt composition. Presented at the 44th Lunar and Planetary Science Conference.
- May, T.W., Wiedmeyer, R.H., 1998. A table of polyatomic interferences in ICP-MS. At. Spectrosc. 19, 150–155.
- Mayhew, L.E., Ellison, E.T., 2020. A synthesis and meta-analysis of the Fe chemistry of serpentinites and serpentine minerals. Philos. Trans. R. Soc. Math. Phys. Eng. Sci. 378, 20180420. <https://doi.org/10.1098/rsta.2018.0420>
- McDonough, W.F., 2014. Compositional model for the Earth's core, in: Holland, H.D., Turekian, K.K. (Eds.), Treatise on Geochemistry. Elsevier, pp. 559–577. <https://doi.org/10.1016/B978-0-08-095975-7.00215-1>

Millet, M.-A., Dauphas, N., Greber, N.D., Burton, K.W., Dale, C.W., Debret, B., Macpherson, C.G., Nowell, G.M., Williams, H.M., 2016. Titanium stable isotope investigation of magmatic processes on the Earth and Moon. *Earth Planet. Sci. Lett.* 449, 197–205. <https://doi.org/10.1016/j.epsl.2016.05.039>

Moynier, F., Le Borgne, M., 2015. High Precision Zinc Isotopic Measurements Applied to Mouse Organs. *J. Vis. Exp.* 52479. <https://doi.org/10.3791/52479>

Murphy, K., Rehkämper, M., Kreissig, K., Coles, B., Van De Fliedrt, T., 2016. Improvements in Cd stable isotope analysis achieved through use of liquid–liquid extraction to remove organic residues from Cd separates obtained by extraction chromatography. *J. Anal. At. Spectrom.* 31, 319–327. <https://doi.org/10.1039/C5JA00115C>

Nier, A.O., 1936. A mass-spectrographic study of the isotopes of argon, potassium, rubidium, zinc and cadmium. *Phys. Rev.* 30, 403–407. <https://doi.org/10.1002/jms.1190300303>

Nisbet, E.G., Arndt, N.T., Bickle, M.J., Cameron, W.E., Chauvel, C., Cheadle, M., Hegner, E., Kyser, T.K., Martin, A., Renner, R., Roedder, E., 1987. Uniquely fresh 2.7 Ga komatiites from the Belingwe greenstone belt, Zimbabwe. *Geology* 15, 1147–1150. [https://doi.org/10.1130/0091-7613\(1987\)15<1147:UFGKFT>2.0.CO;2](https://doi.org/10.1130/0091-7613(1987)15<1147:UFGKFT>2.0.CO;2)

Ohira, I., Jackson, J.M., Sturhahn, W., Finkelstein, G.J., Kawazoe, T., Toellner, T.S., Suzuki, A., Ohtani, E., 2021. The influence of δ -(Al,Fe)OOH on seismic heterogeneities in Earth's lower mantle. *Sci. Rep.* 11, 12036. <https://doi.org/10.1038/s41598-021-91180-9>

Pallavicini, N., Engström, E., Baxter, D.C., Öhlander, B., Ingri, J., Rodushkin, I., 2014. Cadmium isotope ratio measurements in environmental matrices by MC-ICP-MS. *J Anal Spectrom* 29, 1570–1584. <https://doi.org/10.1039/C4JA00125G>

Peng, H., Liu, P., Zheng, H., Belshaw, N.S., Hu, S., Zhu, Z., 2023. Cadmium isotope fractionation during adsorption onto calcite. *Chem. Geol.* 620, 121341. <https://doi.org/10.1016/j.chemgeo.2023.121341>

Pickard, H., Palk, E., Schönbacher, M., Moore, R.E.T., Coles, B.J., Kreissig, K., Nilsson-Kerr, K., Hammond, S.J., Takazawa, E., Hémond, C., Tropper, P., Barfod, D.N., Rehkämper, M., 2022. The cadmium and zinc isotope compositions of the silicate Earth – Implications for terrestrial volatile accretion. *Geochim. Cosmochim. Acta* 338, 165–180. <https://doi.org/10.1016/j.gca.2022.09.041>

Pickard, H., Palk, E., Wood, B.J., Rehkämper, M., 2023. Cadmium isotope fractionation during metal-silicate partitioning – Results and implications for Earth’s volatile accretion. *Chem. Geol.* 618, 121293. <https://doi.org/10.1016/j.chemgeo.2022.121293>

Pringle, E.A., Moynier, F., 2017. Rubidium isotopic composition of the Earth, meteorites, and the Moon: Evidence for the origin of volatile loss during planetary accretion. *Earth Planet. Sci. Lett.* 473, 62–70. <https://doi.org/10.1016/j.epsl.2017.05.033>

Pringle, E.A., Moynier, F., Beck, P., Paniello, R., Hezel, D.C., 2017. The origin of volatile element depletion in early solar system material: Clues from Zn isotopes in chondrules. *Earth Planet. Sci. Lett.* 468, 62–71. <https://doi.org/10.1016/j.epsl.2017.04.002>

Pritzkow, W., Wunderli, S., Vogl, J., Fortunato, G., 2007. The isotope abundances and the atomic weight of cadmium by a metrological approach. *Int. J. Mass Spectrom.* 261, 74–85. <https://doi.org/10.1016/j.ijms.2006.07.026>

Puchtel, I.S., Blichert-Toft, J., Horan, M.F., Touboul, M., Walker, R.J., 2022. The komatiite testimony to ancient mantle heterogeneity. *Chem. Geol.* 594, 120776. <https://doi.org/10.1016/j.chemgeo.2022.120776>

Puchtel, I.S., Blichert-Toft, J., Touboul, M., Horan, M.F., Walker, R.J., 2016. The coupled ^{182}W - ^{142}Nd record of early terrestrial mantle differentiation: Early mantle differentiation. *Geochem. Geophys. Geosystems* 17, 2168–2193. <https://doi.org/10.1002/2016GC006324>

Puchtel, I.S., Blichert-Toft, J., Touboul, M., Walker, R.J., 2018. ^{182}W and HSE constraints from 2.7 Ga komatiites on the heterogeneous nature of the Archean mantle. *Geochim.*

Cosmochim. Acta 228, 1–26. <https://doi.org/10.1016/j.gca.2018.02.030>

Puchtel, I.S., Blichert-Toft, J., Touboul, M., Walker, R.J., Byerly, G.R., Nisbet, E.G., Anhaeusser, C.R., 2013. Insights into early Earth from Barberton komatiites: Evidence from lithophile isotope and trace element systematics. *Geochim. Cosmochim. Acta* 108, 63–90. <https://doi.org/10.1016/j.gca.2013.01.016>

Puchtel, I.S., Hofmann, A.W., Mezger, K., Jochum, K.P., Shchipansky, A.A., Samsonov, A.V., 1998. Oceanic plateau model for continental crustal growth in the Archaean: A case study from the Kostomuksha greenstone belt, NW Baltic Shield. *Earth Planet. Sci. Lett.* 155, 57–74. [https://doi.org/10.1016/S0012-821X\(97\)00202-1](https://doi.org/10.1016/S0012-821X(97)00202-1)

Puchtel, I.S., Humayun, M., 2005. Highly siderophile element geochemistry of 187Os-enriched 2.8 Ga Kostomuksha komatiites, Baltic Shield. *Geochim. Cosmochim. Acta* 69, 1607–1618. <https://doi.org/10.1016/j.gca.2004.09.007>

Puchtel, I.S., Humayun, M., Campbell, A.J., Sproule, R.A., Lesher, C.M., 2004. Platinum group element geochemistry of komatiites from the Alexo and Pyke Hill areas, Ontario, Canada. *Geochim. Cosmochim. Acta* 68, 1361–1383. <https://doi.org/10.1016/j.gca.2003.09.013>

Puchtel, I.S., Walker, R.J., Anhaeusser, C.R., Gruau, G., 2009. Re–Os isotope systematics and HSE abundances of the 3.5 Ga Schapenburg komatiites, South Africa: Hydrous melting or prolonged survival of primordial heterogeneities in the mantle? *Chem. Geol.* 262, 355–369. <https://doi.org/10.1016/j.chemgeo.2009.02.006>

Rehkämper, M., Halliday, A.N., Fitton, J.G., Lee, D.-C., Wieneke, M., Arndt, N.T., 1999. Ir, Ru, Pt, and Pd in basalts and komatiites: new constraints for the geochemical behavior of the platinum-group elements in the mantle. *Geochim. Cosmochim. Acta* 63, 3915–3934. [https://doi.org/10.1016/S0016-7037\(99\)00219-7](https://doi.org/10.1016/S0016-7037(99)00219-7)

Righter, K., Pando, K., Marin, N., Ross, D.K., Righter, M., Danielson, L., Lapen, T.J., Lee, C., 60

2018. Volatile element signatures in the mantles of Earth, Moon, and Mars: Core formation fingerprints from Bi, Cd, In, and Sn. *Meteorit. Planet. Sci.* 53, 284–305. <https://doi.org/10.1111/maps.13005>

Ripperger, S., Rehkämper, M., 2007. Precise determination of cadmium isotope fractionation in seawater by double spike MC-ICPMS. *Geochim. Cosmochim. Acta* 71, 631–642. <https://doi.org/10.1016/j.gca.2006.10.005>

Robson, T.C., Braungardt, C.B., Rieuwerts, J., Worsfold, P., 2014. Cadmium contamination of agricultural soils and crops resulting from sphalerite weathering. *Environ. Pollut.* 184, 283–289. <https://doi.org/10.1016/j.envpol.2013.09.001>

Rosman, Barnes, I.L., Moore, L.J., Gramlich, J.W., 1980a. Isotope composition of Cd, Ca and Mg in the Brownfield chondrite. *Geochem. J.* 14, 269–277. <https://doi.org/10.2343/geochemj.14.269>

Rosman, De Laeter, J.R., 1988. Cadmium mass fractionation in unequilibrated ordinary chondrites. *Earth Planet. Sci. Lett.* 89, 163–169. [https://doi.org/10.1016/0012-821X\(88\)90168-9](https://doi.org/10.1016/0012-821X(88)90168-9)

Rosman, De Laeter, J.R., 1978. A survey of cadmium isotopic abundances. *J. Geophys. Res.* 83, 1279. <https://doi.org/10.1029/JB083iB03p01279>

Rosman, De Laeter, J.R., 1976. Isotopic fractionation in meteoritic cadmium. *Nature* 261, 216–218. <https://doi.org/10.1038/261216a0>

Rosman, De Laeter, J.R., 1975. The isotopic composition of cadmium in terrestrial minerals. *Int. J. Mass Spectrom. Ion Phys.* 16, 385–394. [https://doi.org/10.1016/0020-7381\(75\)85027-3](https://doi.org/10.1016/0020-7381(75)85027-3)

Rosman, De Laeter, J.R., 1974a. The abundance of cadmium and zinc in meteorites. *Geochim. Cosmochim. Acta* 38, 1665–1677. [https://doi.org/10.1016/0016-7037\(74\)90184-7](https://doi.org/10.1016/0016-7037(74)90184-7)

Rosman, De Laeter, J.R., 1974b. Mass spectrometric isotope dilution analyses of cadmium in standard rocks. *Chem. Geol.* 13, 69–74. [https://doi.org/10.1016/0009-2541\(74\)90051-5](https://doi.org/10.1016/0009-2541(74)90051-5)

- Rosman, De Laeter, J.R., Gorton, M.P., 1980b. Cadmium isotope fractionation in fractions of two H3 chondrites. *Earth Planet. Sci. Lett.* 48, 166–170. [https://doi.org/10.1016/0012-821X\(80\)90179-X](https://doi.org/10.1016/0012-821X(80)90179-X)
- Rudge, J.F., Reynolds, B.C., Bourdon, B., 2009. The double spike toolbox. *Chem. Geol.* 265, 420–431. <https://doi.org/10.1016/j.chemgeo.2009.05.010>
- Rudnick, R.L., 1995. Making continental crust. *Nature* 378, 571–578. <https://doi.org/10.1038/378571a0>
- Rudnick, R.L., Gao, S., 2014. Composition of the continental crust, in: Holland, H.D., Turekian, K.K. (Eds.), *Treatise on Geochemistry*. Elsevier, pp. 1–51. <https://doi.org/10.1016/B978-0-08-095975-7.00301-6>
- Sands, D.G., Rosman, K.J.R., De Laeter, J.R., 2001. A preliminary study of cadmium mass fractionation in lunar soils. *Earth Planet. Sci. Lett.* 186, 103–111. [https://doi.org/10.1016/S0012-821X\(01\)00233-3](https://doi.org/10.1016/S0012-821X(01)00233-3)
- Schediwy, S., Rosman, K.J.R., de Laeter, J.R., 2006. Isotope fractionation of cadmium in lunar material. *Earth Planet. Sci. Lett.* 243, 326–335. <https://doi.org/10.1016/j.epsl.2006.01.007>
- Schmitt, A.-D., Galer, S.J.G., Abouchami, W., 2009a. Mass-dependent cadmium isotopic variations in nature with emphasis on the marine environment. *Earth Planet. Sci. Lett.* 277, 262–272. <https://doi.org/10.1016/j.epsl.2008.10.025>
- Schmitt, A.-D., Galer, S.J.G., Abouchami, W., 2009b. High-precision cadmium stable isotope measurements by double spike thermal ionisation mass spectrometry. *J. Anal. At. Spectrom.* 24, 1079. <https://doi.org/10.1039/b821576f>
- She, J.-X., Kubik, E., Li, W., Moynier, F., 2023. Stable Sn isotope signatures of mid-ocean ridge basalts. *Chem. Geol.* 622, 121347. <https://doi.org/10.1016/j.chemgeo.2023.121347>
- Steenstra, E.S., Dankers, D., Berndt, J., Klemme, S., Matveev, S., van Westrenen, W., 2019. Significant depletion of volatile elements in the mantle of asteroid Vesta due to core formation.

Icarus 317, 669–681. <https://doi.org/10.1016/j.icarus.2018.08.020>

Steenstra, E.S., Seegers, A.X., Putter, R., Berndt, J., Klemme, S., Matveev, S., Bullock, E.S., van Westrenen, W., 2020. Metal-silicate partitioning systematics of siderophile elements at reducing conditions: A new experimental database. *Icarus* 335, 113391. <https://doi.org/10.1016/j.icarus.2019.113391>

Stenvinkel, G., Svensson, E., 1935. Band Spectroscopic Observations of the Isotopes of Zinc and Cadmium. *Nature* 135, 955–955. <https://doi.org/10.1038/135955a0>

Sueoka, T.I.K.L., Lee, I.K., Muramatsu, M., Imamura, S., 1985. Geomechanical properties and engineering classification for decomposed granite soils in Kaduna district, Nigeria. Presented at the international conference on geomechanics in tropical lateritic and saprolitic soils, Brasilia, pp. 175–186.

Svensson, E., 1933. Isotope Effect in the Spectrum of Cadmium Hydride. *Nature* 131, 28–28. <https://doi.org/10.1038/131028c0>

Tamblyn, R., Hermann, J., Hasterok, D., Sossi, P., Pettke, T., Chatterjee, S., 2023. Hydrated komatiites as a source of water for TTG formation in the Archean. *Earth Planet. Sci. Lett.* 603, 117982. <https://doi.org/10.1016/j.epsl.2022.117982>

Tan, D., Zhu, J.-M., Wang, X., Han, G., Lu, Z., Xu, W., 2020. High-sensitivity determination of Cd isotopes in low-Cd geological samples by double spike MC-ICP-MS. *J. Anal. At. Spectrom.* 35, 713–727. <https://doi.org/10.1039/C9JA00397E>

Teng, F.-Z., Dauphas, N., Helz, R.T., 2008. Iron Isotope Fractionation During Magmatic Differentiation in Kilauea Iki Lava Lake. *Science* 320, 1620–1622. <https://doi.org/10.1126/science.1157166>

Tugrul, A., Gurpinar, O., 1997. The effect of chemical weathering on the engineering properties of eocene basalts in northeastern Turkey. *Environ. Eng. Geosci.* 3, 225–234. <https://doi.org/10.2113/gseegeosci.III.2.225>

- Van Keken, P.E., Hauri, E.H., Ballentine, C.J., 2002. Mantle mixing: the generation, preservation, and destruction of chemical heterogeneity. *Annu. Rev. Earth Planet. Sci.* 30, 493–525. <https://doi.org/10.1146/annurev.earth.30.091201.141236>
- Van Kooten, E., Moynier, F., 2019. Zinc isotope analyses of singularly small samples (<5 ng Zn): Investigating chondrule-matrix complementarity in Leoville. *Geochim. Cosmochim. Acta* 261, 248–268. <https://doi.org/10.1016/j.gca.2019.07.022>
- Vlastelic, I., Piro, J., 2022. Volatilisation of trace elements during evaporation to dryness of HF-dissolved silicates (BHVO-2, AGV-1, BIR-1, UB-N): open- versus closed-system conditions. *Geostand. Geoanalytical Res.* 46, 519–534. <https://doi.org/10.1111/ggr.12428>
- Wang, H.S., Lineweaver, C., Ireland, T., 2018. The elemental abundances (with uncertainties) of the most Earth-like planet. *Icarus* 299, 460–474. <https://doi.org/10.1016/j.icarus.2017.08.024>
- Wang, Z., Becker, H., Wombacher, F., 2015. Mass fractions of S, Cu, Se, Mo, Ag, Cd, In, Te, Ba, Sm, W, Tl and Bi in geological reference materials and selected carbonaceous chondrites determined by isotope dilution ICP-MS. *Geostand. Geoanalytical Res.* 39, 185–208. <https://doi.org/10.1111/j.1751-908X.2014.00312.x>
- Wang, Z., Laurenz, V., Petitgirard, S., Becker, H., 2016. Earth's moderately volatile element composition may not be chondritic: Evidence from In, Cd and Zn. *Earth Planet. Sci. Lett.* 435, 136–146. <https://doi.org/10.1016/j.epsl.2015.12.012>
- Wasylenki, L.E., Swihart, J.W., Romaniello, S.J., 2014. Cadmium isotope fractionation during adsorption to Mn oxyhydroxide at low and high ionic strength. *Geochim. Cosmochim. Acta* 140, 212–226. <https://doi.org/10.1016/j.gca.2014.05.007>
- Wen, H., Zhang, Y., Cloquet, C., Zhu, C., Fan, H., Luo, C., 2015. Tracing sources of pollution in soils from the Jinding Pb–Zn mining district in China using cadmium and lead isotopes. *Appl. Geochem.* 52, 147–154. <https://doi.org/10.1016/j.apgeochem.2014.11.025>

Willbold, M., Elliott, T., 2017. Molybdenum isotope variations in magmatic rocks. *Chem. Geol.* 449, 253–268. <https://doi.org/10.1016/j.chemgeo.2016.12.011>

Willbold, M., Hibbert, K., Lai, Y.-J., Freymuth, H., Hin, R.C., Coath, C., Vils, F., Elliott, T., 2016. High-precision mass-dependent molybdenum isotope variations in magmatic rocks determined by double-spike MC-ICP-MS. *Geostand. Geoanalytical Res.* n/a-n/a. <https://doi.org/10.1111/ggr.12109>

Witt-Eickschen, G., Palme, H., O'Neill, H.St.C., Allen, C.M., 2009. The geochemistry of the volatile trace elements As, Cd, Ga, In and Sn in the Earth's mantle: New evidence from in situ analyses of mantle xenoliths. *Geochim. Cosmochim. Acta* 73, 1755–1778. <https://doi.org/10.1016/j.gca.2008.12.013>

Wombacher, F., Rehkämper, M., Mezger, K., 2004. Determination of the mass-dependence of cadmium isotope fractionation during evaporation. *Geochim. Cosmochim. Acta* 68, 2349–2357. <https://doi.org/10.1016/j.gca.2003.12.013>

Wombacher, F., Rehkämper, M., Mezger, K., Bischoff, A., Münker, C., 2008. Cadmium stable isotope cosmochemistry. *Geochim. Cosmochim. Acta* 72, 646–667. <https://doi.org/10.1016/j.gca.2007.10.024>

Wombacher, F., Rehkämper, M., Mezger, K., Münker, C., 2003. Stable isotope compositions of cadmium in geological materials and meteorites determined by multiple-collector ICPMS. *Geochim. Cosmochim. Acta* 67, 4639–4654. [https://doi.org/10.1016/S0016-7037\(03\)00389-2](https://doi.org/10.1016/S0016-7037(03)00389-2)

Wood, B.J., Kiseeva, E.S., Mirolo, F.J., 2014. Accretion and core formation: The effects of sulfur on metal–silicate partition coefficients. *Geochim. Cosmochim. Acta* 145, 248–267. <https://doi.org/10.1016/j.gca.2014.09.002>

Wood, B.J., Smythe, D.J., Harrison, T., 2019. The condensation temperatures of the elements: A reappraisal. *Am. Mineral.* 104, 844–856. <https://doi.org/10.2138/am-2019-6852CCBY>

Wood, D.A., Tarney, J., Varet, J., Saunders, A.D., Bougault, H., Joron, J.L., Treuil, M., Cann, 65

J.R., 1979. Geochemistry of basalts drilled in the North Atlantic by IPOD Leg 49: Implications for mantle heterogeneity. *Earth Planet. Sci. Lett.* 42, 77–97. [https://doi.org/10.1016/0012-821X\(79\)90192-4](https://doi.org/10.1016/0012-821X(79)90192-4)

Xie, R.C., Rehkämper, M., Grasse, P., Van De Flierdt, T., Frank, M., Xue, Z., 2019. Isotopic evidence for complex biogeochemical cycling of Cd in the eastern tropical South Pacific. *Earth Planet. Sci. Lett.* 512, 134–146. <https://doi.org/10.1016/j.epsl.2019.02.001>

Xu, Q., Guo, W., Jin, L., Guo, Q., Hu, S., 2015. Determination of cadmium in geological samples by aerosol dilution ICP-MS after inverse aqua regia extraction. *J. Anal. At. Spectrom.* 30, 2010–2016. <https://doi.org/10.1039/C5JA00182J>

Yi, W., Halliday, A.N., Alt, J.C., Lee, D.-C., Rehkämper, M., Garcia, M.O., Langmuir, C.H., Su, Y., 2000. Cadmium, indium, tin, tellurium, and sulfur in oceanic basalts: Implications for chalcophile element fractionation in the Earth. *J. Geophys. Res. Solid Earth* 105, 18927–18948. <https://doi.org/10.1029/2000JB900152>

Yoder, C.F., 1995. Astrometric and geodetic properties of Earth and the solar system, in: Ahrens, T.J. (Ed.), *Global Earth Physics - A Handbook of Physical Constants*, AGU Reference Shelf. American geophysical union, Washington, D. C., pp. 1–31. <https://doi.org/10.1029/RF001p0001>

Zhang, Y., Wen, H., Zhu, C., Fan, H., Luo, C., Liu, J., Cloquet, C., 2016. Cd isotope fractionation during simulated and natural weathering. *Environ. Pollut.* 216, 9–17. <https://doi.org/10.1016/j.envpol.2016.04.060>

Zhou, D., Cao, S., Liu, J., Li, X., Dong, Y., Neubauer, F., Bai, J., Li, H., 2022. Carbonation and serpentinization of diopside in the Altun Mountains, NW China. *Sci. Rep.* 12, 21361. <https://doi.org/10.1038/s41598-022-25612-5>

Zhu, C., Wen, H., Zhang, Y., Yin, R., Cloquet, C., 2018. Cd isotope fractionation during sulfide mineral weathering in the Fule Zn-Pb-Cd deposit, Yunnan Province, Southwest China. *Sci.*

Total Environ. 616–617, 64–72. <https://doi.org/10.1016/j.scitotenv.2017.10.293>